NREL/TP-425-6344 • UC Category: 335 • DE94006948

Injector Spray Characterization of Methanol in Reciprocating Engines

L. Dodge
D. Naegeli
Southwest Research Institute
San Antonio, Texas

NREL technical monitor:
C. Colucci

National Renewable Energy Laboratory
1617 Cole Boulevard
Golden, Colorado 80401-3393
A national laboratory of the U.S. Department of Energy
Operated by Midwest Research Institute
for the U.S. Department of Energy
Under Contract No. DE-AC02-83CH10093

Prepared under Subcontract Number AW-2-12266-1

June 1994

NOTICE

Printed in the United States of America
Available from:
National Technical Information Service
U.S. Department of Commerce
5285 Port Royal Road
Springfield, VA 22161

Price: Microfiche A01
Printed Copy A04

Codes are used for pricing all publications. The code is determined by the number of pages in the publication. Information pertaining to the pricing codes can be found in the current issue of the following publications which are generally available in most libraries: *Energy Research Abstracts (ERA)*; *Government Reports Announcements and Index (GRA and I)*; *Scientific and Technical Abstract Reports (STAR)*; and publication NTIS-PR-360 available from NTIS at the above address.

Printed on recycled paper

Preface

This work was conducted by Southwest Research Institute (SwRI), San Antonio, Texas, under Subcontract No. AW-2-12266-1, Prime Contract No. DE-AC02-83CH10093, SwRI Project No. 03-5299 for the National Renewable Energy Laboratory (NREL), Golden, Colorado, and the U.S. Department of Energy (DOE), Washington, D.C. The contributions of technical monitors Brent K. Bailey and Christopher P. Colucci of NREL, John A. Russell of DOE, and subcontract administrator Ernest G. Oster of NREL are gratefully acknowledged. Further, contributions from the Musashi Institute of Technology (Musashi I.T.) in Tokyo, Japan, were essential to the conduct of Task 3, Hydrogen-Air Mixing Evaluation. The contributions of Katsuyoshi Koyanagi, Kimitaka Yamane, and Shoichi Furuhama are gratefully acknowledged. Susuma Ariga of SwRI helped to make the interaction with Musashi I.T. possible. Douglas Leone is greatly appreciated for his help in setting up the personal computer version of Chemkin-II, which was used in the chemical kinetics modeling work in Task 2, Injector-Spray Characterization of Methanol. The patience and expertise of Ms. Janie Gonzalez in preparing this report are appreciated.

This effort consisted of three fairly autonomous tasks. The first task addressed cold-starting problems in alcohol-fueled, spark-ignition engines by using fine-spray port-fuel injectors to inject fuel directly into the cylinder. This task included development and characterization of some very fine-spray, port-fuel injectors for a methanol-fueled spark-ignition engine. After determining the spray characteristics, a computational study was performed to estimate the evaporation rate of the methanol fuel spray under cold-starting conditions and steady-state conditions. The second task was to perform a fundamental kinetic study of the autoignition characteristics of methylal, an oxygenated fuel that produces almost no soot in diesel engines, but, in contrast with most oxygenated fuels, has an excellent cetane number. The third task was to perform a computational study of fuel-air mixing in a hydrogen jet using a spark-ignited, hydrogen-fueled engine. The computational results were compared with experimental measurements being conducted at Musashi I.T. The hydrogen-air mixing work was directed at understanding the extreme sensitivity of ignition to spark plug location and spark timing in direct-injected, hydrogen-fueled engines.

The first task is discussed in this report. Tasks 2 and 3 are covered in NREL reports TP-425-6345 and TP-425-6346, respectively.

Executive Summary

Methanol is an attractive alternative fuel for spark-ignition engines because it has an octane number well above 100 and produces emissions with a significantly lower reactivity factor than gasoline (about 0.41 versus 1.0). Methanol may be derived from natural gas or coal. A significant problem associated with the use of methanol in spark-ignition engines is the low-temperature, cold-starting problem caused by the low vapor pressure and high heat of vaporization of methanol. The advantages and disadvantages of ethanol are similar to those for methanol, except that ethanol is a renewable fuel that can be made from biological sources, while methanol is not a renewable fuel. However, methanol is approximately cost competitive with gasoline, while ethanol is currently more expensive than gasoline.

In this project, a new concept is proposed to reduce the low-temperature, cold-starting difficulties of alcohol-fueled vehicles. This concept also is intended to improve emissions in alcohol-fueled engines when engine and air temperatures are low. The approach is to use fine-spray, port-fuel injectors to produce drops small enough to follow the airstream past the intake valves and into the engine cylinders. The spray drops would be fine enough to stay suspended in the air as it goes into the cylinder, in contrast with conventional port-fuel injectors that spray fuel drops onto surfaces in the intake valve and port. In these conventional systems, it is mostly fuel vapor, not liquid fuel, that goes into the cylinder during cranking. For fuel drops to follow the airstream, the drops must be roughly 20 μm in diameter or smaller. To follow up on this new cranking and starting concept, we developed fine-spray fuel injectors, and used a computer model to estimate the performance of fine alcohol fuel sprays in engines. The goal for the fuel injector design was to produce a significant amount of the spray with drop sizes smaller than 20 μm. Sauter mean diameter (SMD) is a commonly used average drop size in combustion studies, and we set an SMD goal of 10 μm to produce a significant fraction of spray drops smaller than 20 μm.

Air-assist caps fitted onto standard pintle or multi-hole port-fuel injectors were developed and tested on methanol (M100) fuels. These injectors exceeded the goal of producing sprays with SMDs less than 10 μm using air pressure differentials of 138 $kPa_{diff.}$ (20 psid, d = differential) or less. Using a 1.4-mm exit hole diameter and 100 $kPa_{diff.}$ (15 psid) pressure differential from an air-assist injector cap, cross-section average SMDs of about 7.5 μm were produced with fuel-injection pulse widths of 4 ms (idle condition) and SMDs of 9 μm were produced with a 10-ms pulse width. Standard production pulse-width modulation can be used for fuel control with these injectors, although the engine controller may need to account for air flow into the engine through the injector, depending on the engine control strategy.

A detailed spray evaporation model developed at SwRI, the Trajectory and Evaporation of Spray Systems (TESS) code, was combined with an engine cycle-simulation model to predict in-cylinder temperatures, pressures, evaporation rates, and combustion rates. Calculations of in-cylinder evaporation of methanol (M100) and ethanol (E100) were compared with a single-component simulation of gasoline, n-heptane, at cranking temperatures from -25°C to 25°C and at road-load condition. During cranking, the n-heptane produced a prevaporized combustible fuel-air mixture by top-dead-center (TDC) of the compression stroke for all temperatures, while the evaporation rates of ethanol and methanol were lower due to their higher latent heats of vaporization (n-heptane, 318 kJ/kg; ethanol, 963 kJ/kg; methanol, 1121 kJ/kg). At the highest temperature of 25°C, the alcohols could produce a prevaporized vapor-air combustible mixture; at the lowest temperature of -25°C, the vaporization of the alcohols appeared too slow to get a prevaporized combustible mixture. However, it is proposed that if the fine spray could be kept suspended in the air, it would be possible to use direct-spark vaporization and combustion of the liquid drops. Engine tests are required to evaluate this concept.

The computer modeling of spray evaporation revealed some further interesting aspects of in-cylinder fuel spray evaporation. Drop evaporation times scale approximately with the square of the drop diameter, so a reduction by a factor of ten in drop size reduces evaporation rates by a factor of 100. This is true for

the methanol sprays evaporating in-cylinder until the SMD reaches about 10 μm. At this size and below, the evaporation is so fast that the methanol fuel vapor saturates the air in the cylinder almost instantaneously at cranking conditions for the temperatures available at any given crank angle. This occurs for all crank angles during the air intake stroke and during the compression stroke. Therefore, for methanol sprays, further reductions in drop sizes below SMDs of about 10 μm will not increase evaporation rates. The same conclusion may be drawn for ethanol sprays—reductions in drop size down to SMDs of about 10 μm increase evaporation rates in-cylinder, but further reductions do not significantly increase evaporation rates. For heptane (simulating gasoline), the fuel vapor for sprays of 10 μm SMD saturates the in-cylinder gases during the intake stroke but not on the combustion stroke. Because the evaporation of heptane is almost complete during the intake stroke, sprays finer than 10 μm SMD are only significant during the compression stoke. All of the above discussion concerns drop size effects on evaporation rates. In contrast to the 10 μm limit for evaporation rate of the alcohol fuels, reductions in drop size below 10 μm are effective in increasing the fraction of drops that will follow the air flow from a port-fuel injector into the cylinder.

Another observation from the modeling work is the effect of enrichment on providing a prevaporized combustible mixture at TDC (or slightly before) on the compression stroke of a cranking engine. For the heptane fuel, enriching the injected-fuel mixture from stoichiometric to twice stoichiometric increases the prevaporized fuel at TDC by a factor of almost two. In contrast, enriching a neat methanol mixture in-cylinder from stoichiometric to twice stoichiometric does not increase the prevaporized fuel at all. A stoichiometric mixture of methanol absorbs all available enthalpy in the cylinder and further amounts of liquid fuel do not increase the amount of vapor. The effect of enrichment for ethanol is between that of heptane and methanol. Increasing the amount of liquid fuel injected into the cylinder from stoichiometric to twice stoichiometric increases the fuel vapor at TDC by only about 23%. The practical implication of these results is as follows. Enrichment for cranking is normally used to increase the amount of fuel light ends that can be evaporated and ingested into the engine. For alcohol blends that include gasoline or other vapor enhancers, this approach is still effective. However, as vapor-enhancing additives in alcohol fuels are reduced, the advantages of enrichment for cold-starting become much less than for gasoline. For neat methanol, the only advantage of enrichment at cold-starting is to offset fuel lost in the intake system so that a combustible mixture of liquid fuel is obtained in-cylinder and the fuel may be evaporated or spark-ignited as a liquid spray.

Another approach to enhancing cold-startability of alcohol-fueled engines is to increase the compression ratio. This increases compression heating of the gas and thereby increases the amount of fuel spray evaporation. Again, this approach was evaluated with the TESS code combined with the cycle simulation. From a baseline compression ratio of 9.3, increasing the compression ratio to 12.0 and using a fine-spray fuel injector with an SMD of 10 μm increases the predicted evaporated fuel at TDC by less than 10% for both methanol and ethanol. Thus, while increasing the compression ratio should increase cycle efficiency significantly, the improvement in cold-startability will be slight.

Contents

List of Figures

List of Figures
(Continued)

List of Figures
(Continued)

List of Figures
(Concluded)

Injector Spray Characterization of Methanol in Reciprocating Engines

Background

Almost all spark-ignition engines currently in production use either throttle-body or port-fuel injection to deliver fuel to the cylinder. This is done with precise electronic control of fuel-flow rates by pulse width modulation (PWM) based on feedback from an oxygen sensor in the exhaust. Fuel is not sprayed directly into the cylinders, but is sprayed into the intake system. After the fuel vaporizes, the fuel vapor is transported into the cylinder along with some liquid fuel. The liquid fuel transported into the cylinder is not usually in the form of drops as sprayed from the fuel injector, but rather liquid traveling along the intake valve or the walls of the intake port. Thus, the manifold and port walls act as prevaporizers for the fuel that is sprayed onto the intake valve(s). These systems perform reasonably well after engine and catalyst warmup, with low emissions due to efficient catalyst operation by controlling the fuel-air ratio near stoichiometric. Port-fuel injection is more expensive than throttle-body injection, but port injection can maintain tighter fuel-air ratio control because less fuel is deposited in the intake manifold.

Although current engines perform fairly well when warm, engine performance and emissions typically suffer during cold-starts (and sometimes hot-starts) and during transient operation. During cold-starts, the prevaporizing is severely hampered by the low temperature walls. To get sufficient fuel into the cylinder for combustion, fuel is enriched so that the light ends of the fuel, the only ones to vaporize off the cold surfaces, are in sufficient concentration to provide combustion and power. However, this leaves the heavy ends in the intake system; they vaporize and enter the cylinder in a somewhat uncontrolled fashion that can be only partially corrected by the oxygen measurement feedback system. The liquid fuel traveling along the walls also enters the cylinder in a somewhat erratic fashion.

Transient accelerations also are a problem with these prevaporizing systems. Because it may take several engine cycles to prevaporize the fuel, the engine will be fuel-lean during accelerations unless extra fuel (transient compensation) is provided so that the light ends from the extra fuel are sufficient to provide a stoichiometric mixture in the cylinder. The heavier ends of this extra fuel in the intake system then will come into the cylinder at a later time, again making fuel-air control difficult. On deceleration, the lower intake manifold pressures tend to flash vaporize some of the fuel in the intake system. This, combined with the reduced air flow during decelerations, usually leads to fuel-rich spikes in the fuel-air ratio.

Alcohol fuels such as methanol and ethanol vaporize more slowly than the light ends in gasoline, making low-temperature cold-starting impossible and transient compensation difficult. Therefore, light ends from gasoline are typically added to the alcohol fuels at a level of about 15% for methanol (M85) and about 20% for ethanol (called E85, ignoring the 5% denaturant gasoline used in the "pure" ethanol). These alcohol/gasoline blends typically do not start as well as neat (pure) gasoline at low temperatures, but are a dramatic improvement over neat alcohol fuels. The addition of light ends to the alcohol fuels is not without demerits. The naturally low vapor pressure, and therefore evaporative emissions, of the alcohol fuels are lost with the addition of light ends. In flexible-fuel vehicles where alcohol content may vary from 0% to 85% of the fuel mix, very high vapor pressures are encountered with small amounts of alcohol in gasoline (about 10%) because of the non-ideal nature of the blend. In addition to helping with low-temperature cold-starting, the addition of light ends to methanol fuel helps improve flame luminosity (in the case of fuel fires) and reduces fuel tank ullage flammability. However, the gasoline addition increases problems of phase separation with water absorption and probably increases smog production.

Alcohols also have a much higher heat of vaporization than gasoline. Thus, their evaporation cools the intake air charge considerably more than does gasoline, as will be demonstrated later. This slightly improves cycle efficiency by reducing compression work and can also improve volumetric efficiency and

peak power if the evaporation occurs before intake-valve closing. However, the high latent heat of vaporization makes cold-starting more difficult by limiting evaporation of the fuel.

Direct in-cylinder fuel injection has been used with neat methanol-fueled (i.e., M100) engines to overcome low-temperature, cold-starting problems (Siewert and Groff 1987). However, there are few spark-ignition engines in the current marketplace with cylinder heads and combustion chambers designed to accommodate direct injection. Current market projections for alcohol-fueled engines make complete engine redesign to accommodate alcohol fuels impractical. Switching from port or throttle-body fuel injectors to direct in-cylinder injectors requires a complete rethinking and remapping of engine performance and emissions strategies. The ideal solution for the alcohol-fueled engine would involve overcoming the low-temperature, cold-start, and transient compensation problems using an alcohol fuel with minimum volatility enhancers and minimum modifications to existing engine design.

Objective

The objective of this work was to demonstrate a new concept in fuel injection for alcohol-fueled spark-ignition engines—the use of modified port-fuel injectors to inject fuel directly past the intake valves and into the cylinder, avoiding fuel deposition and prevaporization in the intake manifold/port. This required demonstration that fine-spray methanol port-fuel injectors could be developed that would produce a fine enough spray that a significant portion of the spray would follow the airstream directly into the cylinder. This technique for low-temperature cold-starting would not depend on prevaporization of the fuel in the intake manifold/port. Further, these fuel injectors should be compatible with conventional PWM-type fuel control systems.

The concept of "direct injection" of alcohol fuels into the cylinder from port-fuel injectors was to be evaluated through the use of computer models to determine the impact on cold-starting and overall engine performance.

Approach

The approach to meeting the above objective involved both experimental and computational work. The experimental approach to developing a fine-spray injector compatible with PWM control was to fit an internal-mix, air-assist, fuel-air mixing cap onto a convention pintle injector. Thus, the conventional PWM control could be used to control fuel flow through the standard pintle injector, while the air-assist mixing cap could produce a very fine spray. The Trajectory and Evaporation of Spray Systems (TESS) computer model was used to help determine how fine a spray was required for the fuel drops to stay suspended in the airstream as they passed the intake valve.

To evaluate the expected performance for direct injection of alcohol fuels from a port-fuel injector, two existing computer models at SwRI were combined. A fairly standard internal-combustion engine cycle-simulation model developed at SwRI was combined with the TESS spray code so that the alcohol fuel spray evaporation could be estimated during the complete engine cycle.

Development of Fine-Spray Fuel Injectors

Fuel-Spray Facilities

SwRI has two laboratories for determining spray characteristics of various types of atomizers. One is called the Low-Turbulence, Atmospheric Pressure Spray Laboratory; the major features are shown schematically in Figure 1. Air is pulled by an explosion-proof fan through a bell mouth, through

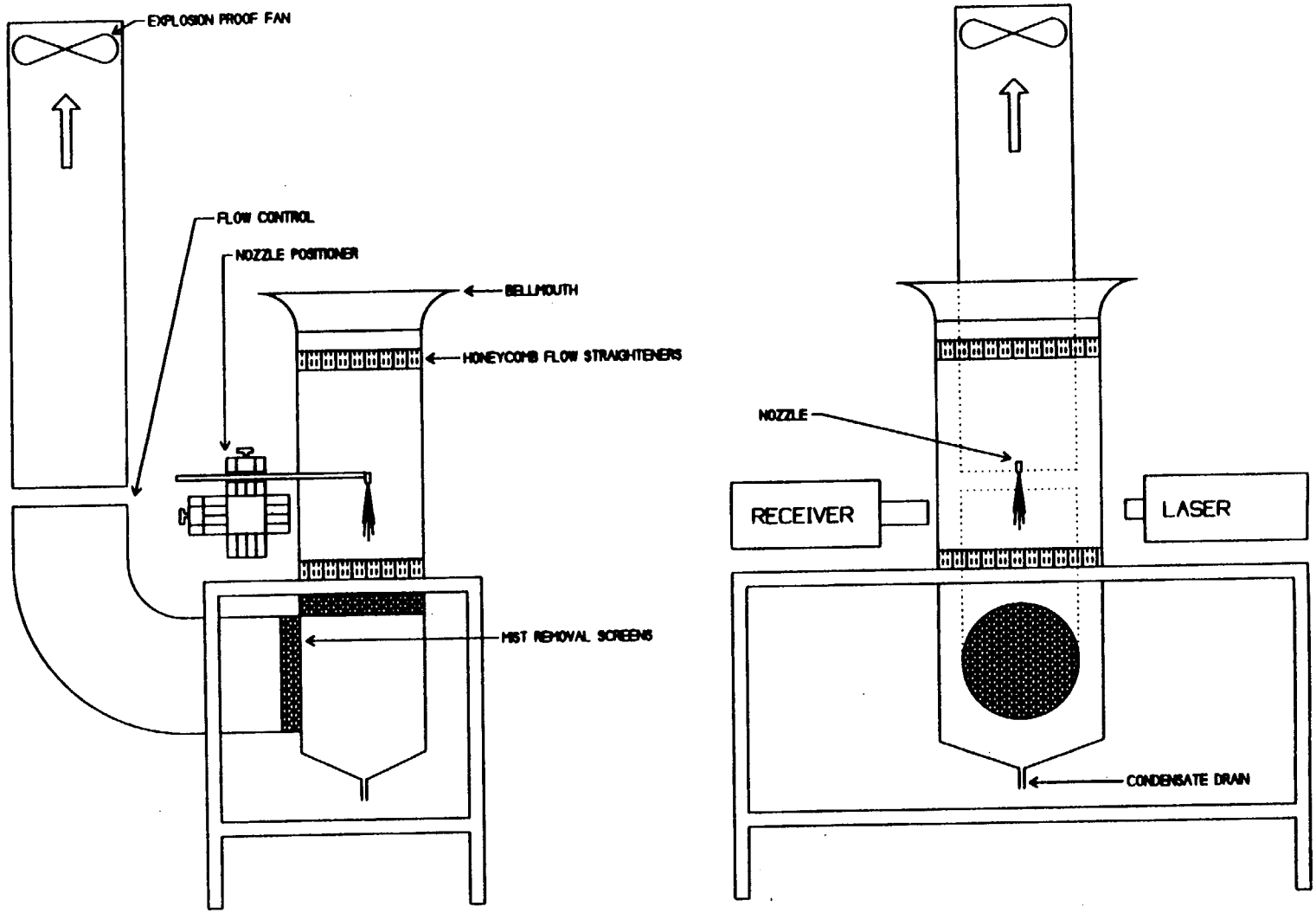

Figure 1. Atmospheric-pressure low-turbulence spray chamber with computer-controlled nozzle positioner.

honeycomb flow straighteners, through the test section, through another set of honeycomb flow straighteners, through chilled screens to condense and remove the fuel spray, and finally through the fan where the air is exhausted to the atmosphere. Air flow in the test section has a velocity of about 0.9 m/s and a turbulence intensity of less than 2%. A two-dimensional, computer-controlled traversing system is capable of accurately positioning spray nozzles so that spray measurements may be made repeatably at various axial and radial locations.

The second laboratory for spray measurements is the Variable Pressure and Temperature Spray Laboratory. It includes high-pressure compressors that can provide elevated air pressures for spray measurements from 101 kPa (1 atm.) to 1515 kPa (15 atm.) or can be used as a power source for an air ejector to provide subatmospheric pressures from 101 kPa (1 atm.) to 25 kPa (0.25 atm.). Air temperatures can be varied from room temperature to 800°C. By using liquid nitrogen, temperatures also can be reduced to -30°C.

Most of the spray tests for this project were conducted at the Variable Pressure and Temperature Spray Laboratory configured with the air ejector to provide subatmospheric pressure atmospheres to simulate the intake manifold of a spark-ignition engine. This configuration is illustrated in Figure 2. Chamber pressures were typically 51 kPa (0.5 atm.), 76 kPa (0.75 atm.), and 101 kPa (1 atm.). This simulation capability is especially useful when testing air-assist injectors, because changing the manifold pressure in an engine changes the atomizing air pressure differential across the injectors as well as the air velocity and air density through the exit orifice. Because of the complexities involved in atomization, it has not been possible previously to predict how air-assist injectors would perform at low manifold pressures and air densities based on tests at atmospheric pressure. With this subatmospheric pressure facility, it is possible to characterize air-assist injectors over their normal operating range in an engine. Inside chamber diameter is about 0.25 m (10 in.). A honeycomb flow straightener (3.2-mm, or 1/8 in., cell diameter) is used upstream of the measurement location to minimize air turbulence.

SwRI has two automated particle-sizing instruments: a Malvern Model 2600 laser-diffraction particle sizer and an Aerometrics phase-Doppler particle analyzer. Only the laser-diffraction instrument was used for these tests. The phase-Doppler instrument does not perform well on very fine, high-velocity sprays produced by air-assist injectors. All drop-size measurements were performed by scanning the spray nozzle continuously across the laser beam so that a complete cross-sectional slice of the spray was sampled (Dodge 1988). Approximately 2000 samples of the spray were recorded and averaged to obtain this cross-section average, which has been shown to properly weight the overall spray characteristics (Dodge 1988). The laser beam diameter was 9 mm, and the 300-mm focal length Fourier transform lens was used for all tests.

All measurements were made at an axial distance of 75 mm from the exit of the air-assist injector cap. Increasing the distance decreases the spray density, which reduces multiple-scattering errors, but increases errors because of evaporation of the spray. Thus, 75 mm was a compromise where multiple-scattering errors were small, but evaporation was limited. No multiple-scattering corrections were made for these data because in using the continuous-scan technique, the extinction of the unscattered light is constantly changing.

All spray measurements were made with neat methanol (M100) at a temperature of 27°C (80°F). Methanol does not contain the light ends that gasoline does and, as a result, did not produce laser-beam wander due to refractive index gradients in the rapidly evaporating spray as gasoline does. All the laser-diffraction data appeared to be of high quality and repeat measurements at each condition showed excellent repeatability. (Two data are shown for each condition in all graphs, although in some cases they appear as a single point because of overlap.)

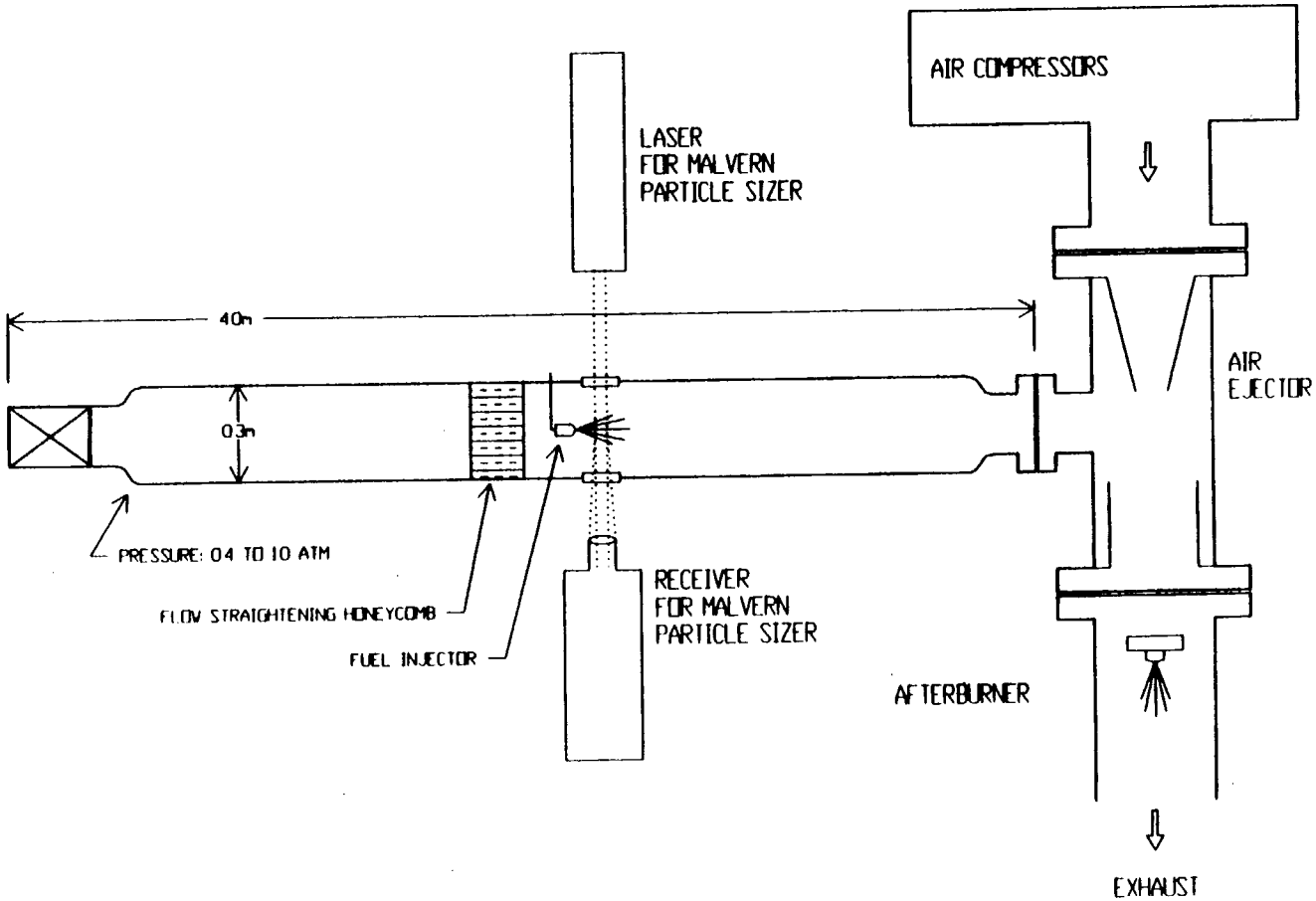

Figure 2. Subatmospheric pressure spray characterization chamber.

Fuel-Injector Design

A narrow-beam pintle fuel injector for a Ford Escort 1.9-L engine was obtained and spray tested. Operating at design operating pressure (300 kPa; 3 atm.) and a temperature of 27°C (80°F) on methanol, an average drop size as represented by the Sauter mean diameter (SMD) was measured to be 116 μm for the 4-ms pulse width (an idle condition) and 136 μm for the 10-ms pulse width (a higher power condition). This injector was converted into three different internal-mix, air-assist injectors by installing three different fuel-air mixing caps on the end of the injector, with exit hole diameters of 1.0 mm, 1.4 mm, and 2.0 mm. The fuel-air mixing caps are shown in Figure 3, and the fit of the caps onto the standard pintle injector is shown in Figure 4. The fuel-air mixing caps are sealed with O-rings on this prototype injector so that the caps can be easily changed.

Fuel-Injector Spray Performance

Fuel pulse widths were set at 4 ms (equivalent to an idle condition) and 10 ms (higher power condition). Atomizing air pressures were 115, 136, 170, 205, and 239 $kPa_{absolute}$, so the differential atomizing air pressures varied with the chamber pressures.

Atomization results as a function of differential air pressure for the 1-mm diameter air cap are shown in Figures 5 and 6 for the 4-ms and 10-ms pulse widths, respectively. Note that at high atomizing pressure, this injector achieves and exceeds the target SMD of 10 μm. This target size is to allow the fuel drops to follow the airstream into the cylinder to achieve cold-start when the temperature is too low to prevaporize a combustible mixture in the intake manifold. Thus, this injector design is successful in achieving and exceeding its goal.

When plotted against atomizing air-mass flow rate, the lower chamber pressures lead to significantly better atomization for a fixed air-mass flow rate, as shown in Figures 7 and 8 for the two different fuel pulse widths. This is due to the higher atomizing air velocities when the chamber pressure is lowered at a fixed air-mass flow rate.

Similar results for the 1.4-mm diameter hole are shown in Figures 9 and 10 for atomization versus differential air pressure, and in Figures 11 and 12 as a function of atomizing air-mass flow rate. Comparison with Figures 5 through 8 indicates that the larger hole size gets better atomization than the smaller hole for a fixed-pressure differential, but with significantly higher air-mass flow rates.

Similar results for the 2-mm diameter hole are shown in Figures 13 and 14 for atomization as a function of differential air pressure, and in Figures 15 and 16 as a function of atomizing air-mass flow rate. Again, the atomization improves with the larger hole size at a given differential pressure, but the air mass flow rates are much higher.

To more directly compare the effect of hole size on atomization, Figures 17 and 18 compare the SMDs versus differential air pressure at a chamber pressure of 101 $kPa_{absolute}$ for fuel injector pulse widths of 4 ms and 10 ms for all three hole sizes. The same type of data for a chamber pressure of 76 kPa (75 atm.) are shown in Figures 19 and 20. These data indicate that the ultimate atomization quality of the 1.4-mm and 2-mm diameter holes are better than the 1-mm diameter hole at high differential air pressures. Because the 1.4-mm hole requires less air flow, it is preferable to the 2-mm diameter hole. The SMDs versus atomizing air flow are shown in Figures 21 and 22 for a chamber pressure of 101 $kPa_{absolute}$ and injector pulse widths of 4 ms and 10 ms. Unfortunately, the highest air-mass flows for the 2-mm hole were off-scale for the rotameter and are not shown.

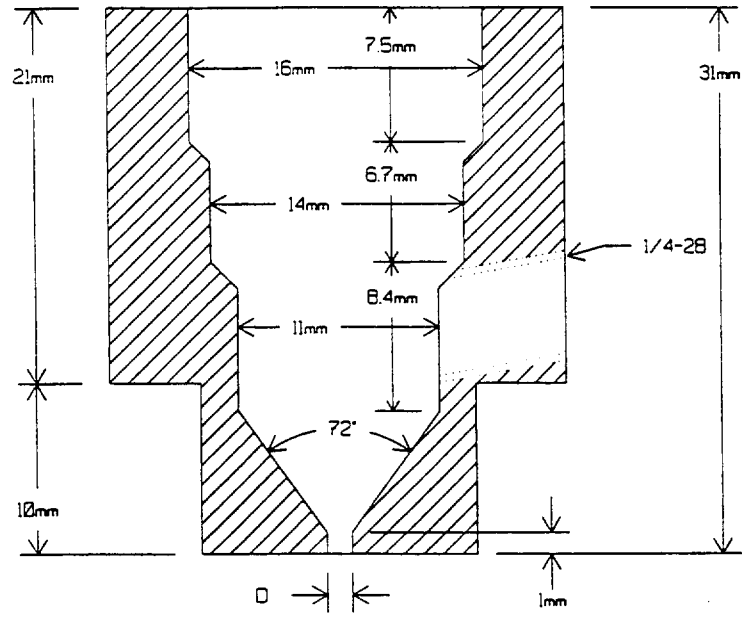

3 INJECTOR CAPS:
D = 1.0mm
D = 1.41mm
D = 2.0mm

Figure 3. SwRI internal-mix, air-assist injector caps.

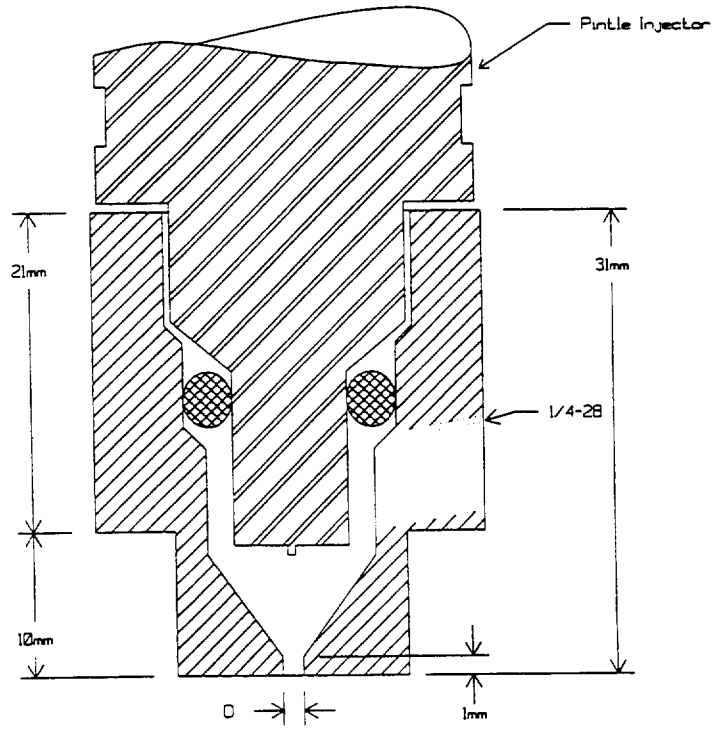

3 INJECTOR CAPS:
D = 1.0mm
D = 1.41mm
D = 2.0mm

Figure 4. SwRI internal-mix, air-assist injector cap mounted on conventional pintle injector.

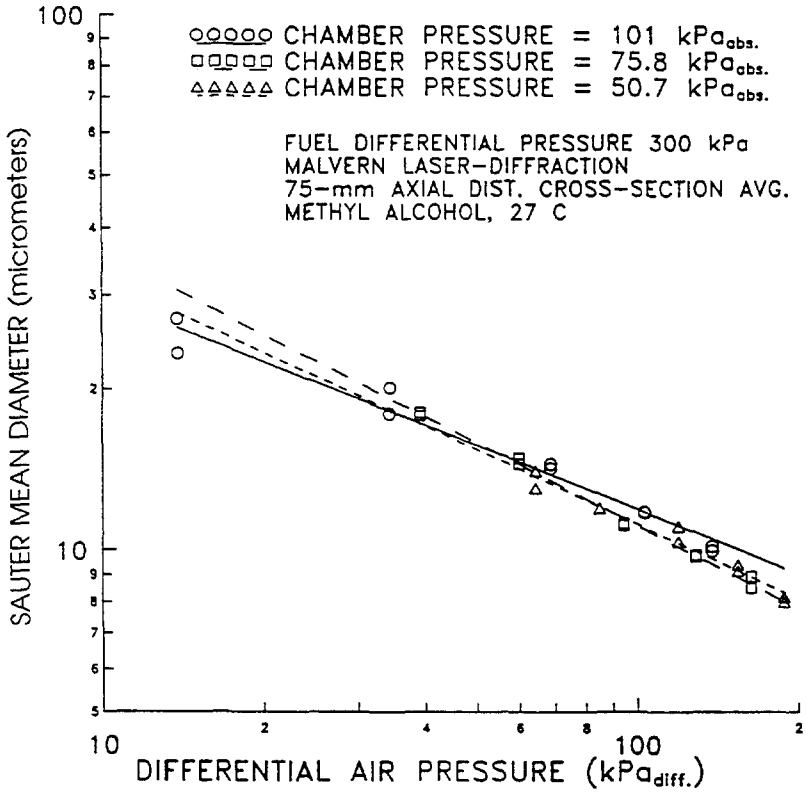

Figure 5. Atomization quality (cross-section average SMD) versus differential air pressure for SwRI 1.0-mm exit-hole diameter, internal-mix, air-assist injector spraying methanol for 4-ms pulse width, 50-ms period.

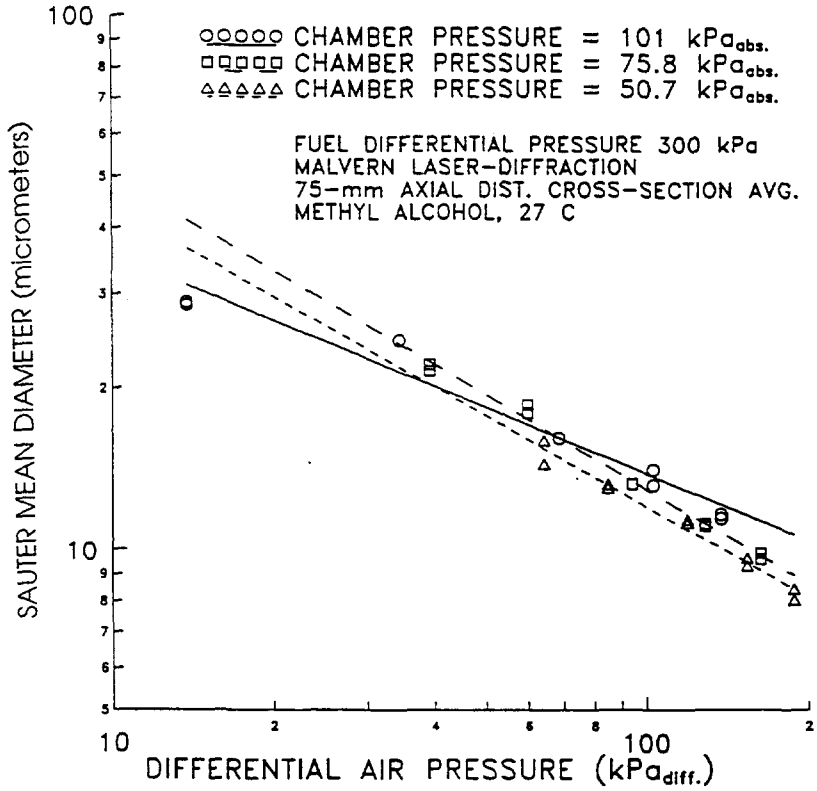

Figure 6. Atomization quality (cross-section average SMD) versus differential air pressure for SwRI 1.0-mm exit-hole diameter, internal-mix, air-assist injector spraying methanol for 10-ms pulse width, 50-ms period.

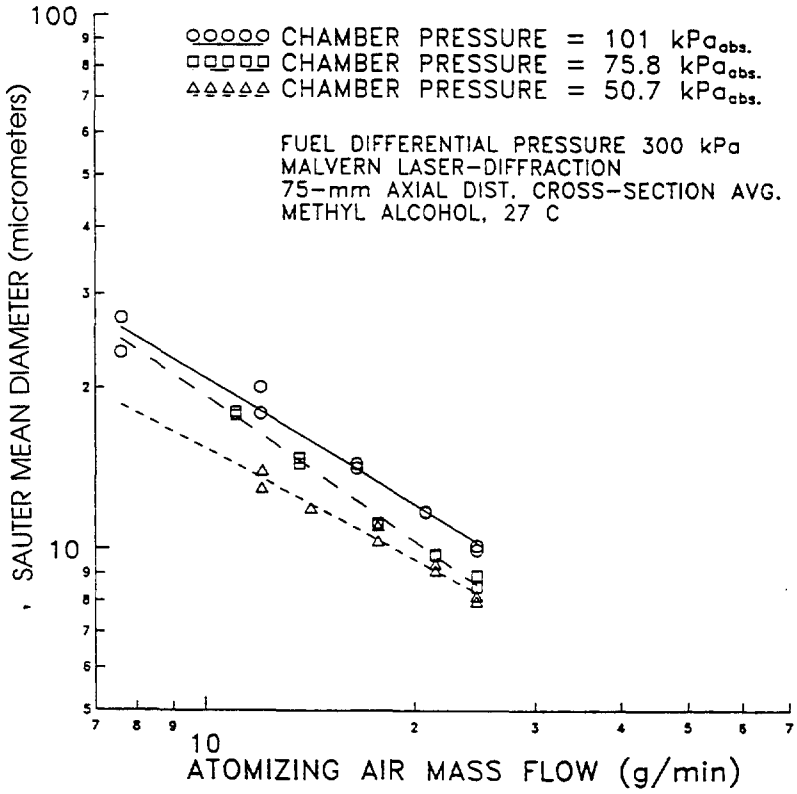

Figure 7. Atomization quality (cross-section average SMD) versus atomizing air flow for SwRI 1.0-mm exit hole diameter, internal-mix, air-assist injector spraying methanol for 4-ms pulse width, 50-ms period.

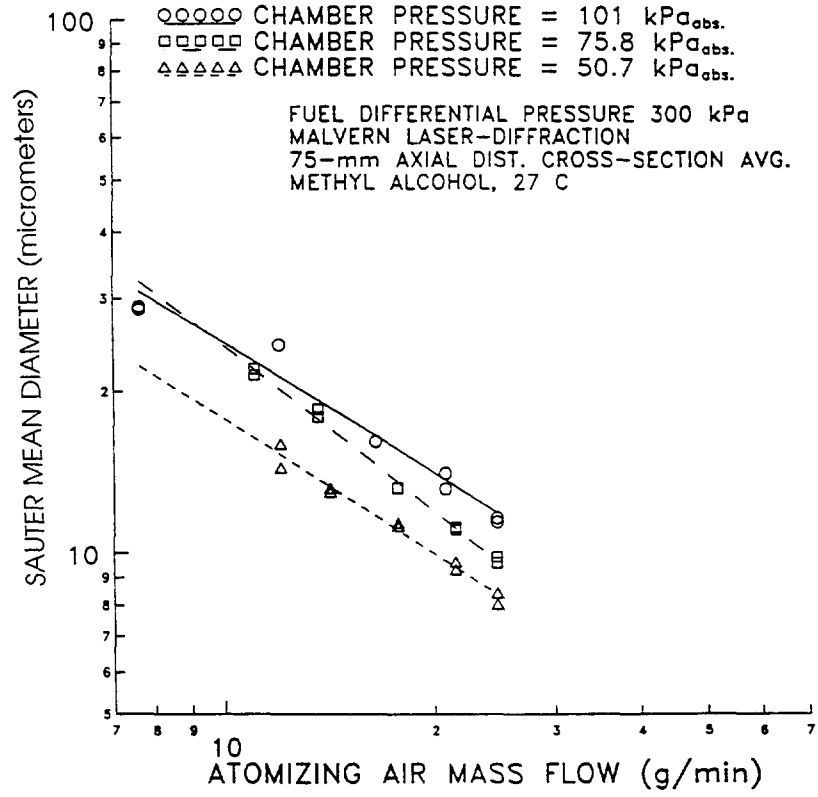

Figure 8. Atomization quality (cross-section average SMD) versus atomizing air flow for SwRI 1.0-mm exit hole diameter, internal-mix, air-assist injector spraying methanol for 10-ms pulse width, 50-ms period.

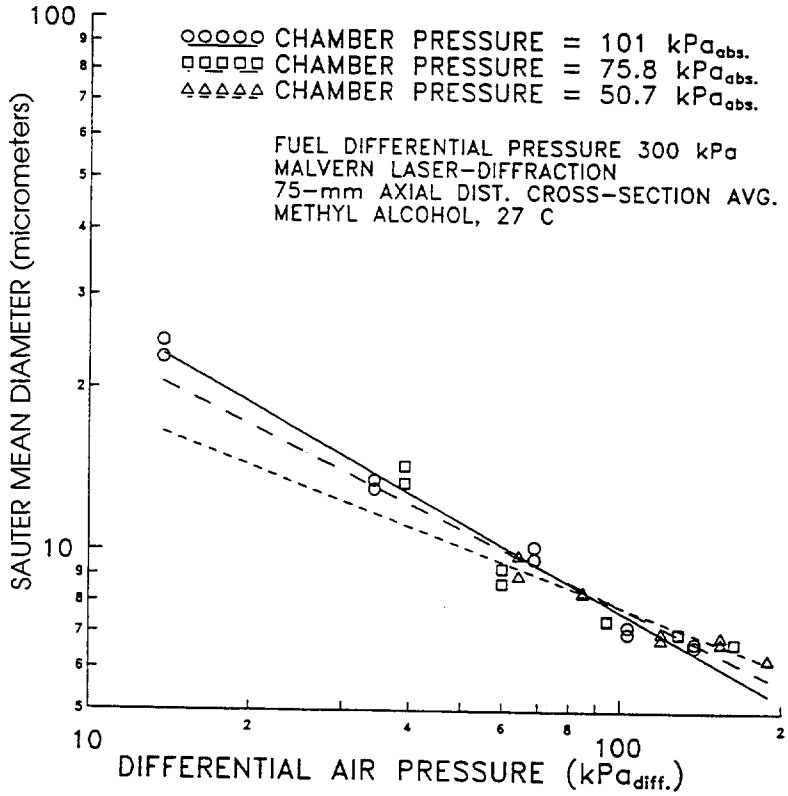

Figure 9. Atomization quality (cross-section average SMD) versus differential air pressure for SwRI 1.4-mm exit hole diameter, internal-mix, air-assist injector spraying methanol for 4-ms pulse width, 50-ms period (same as Figure 5, but 1.4-mm hole diameter).

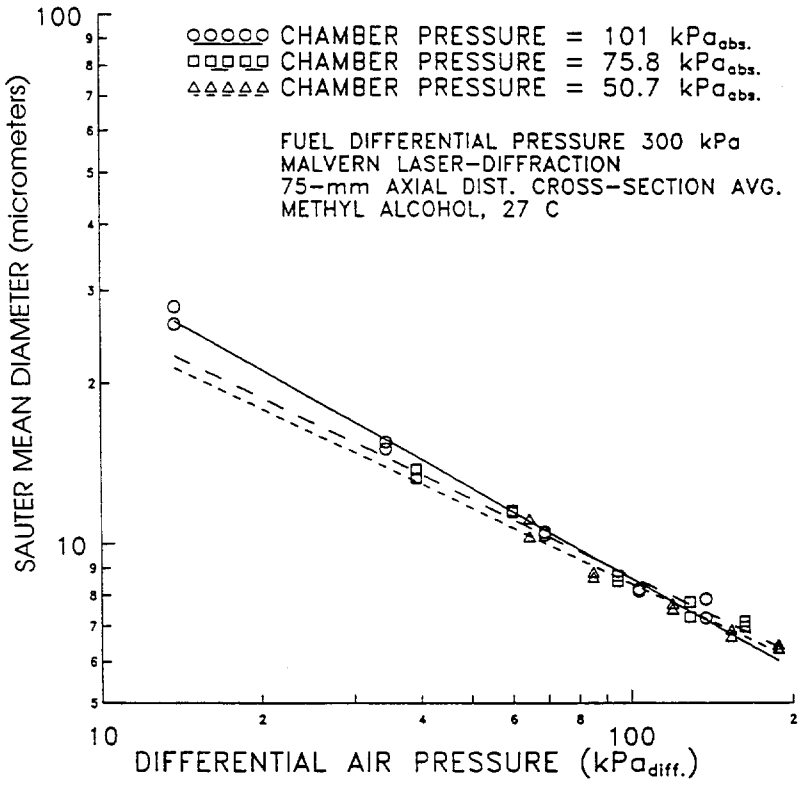

Figure 10. Atomization quality (cross-section average SMD) versus differential air pressure for SwRI 1.4-mm exit hole diameter, internal-mix, air-assist injector spraying methanol for 10-ms pulse width, 50-ms period (same as Figure 6, but 1.4-mm hole diameter).

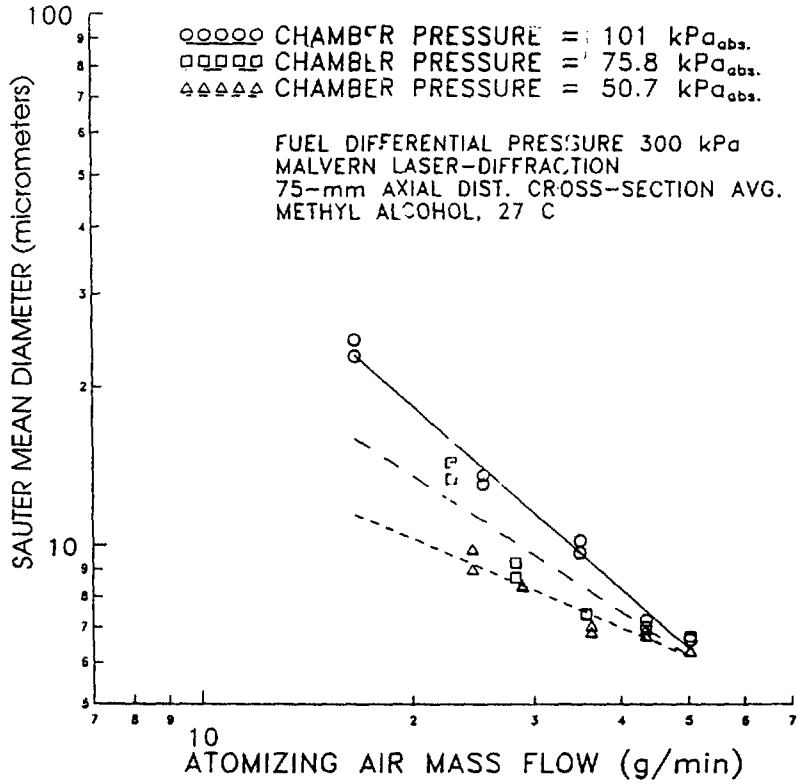

Figure 11. Atomization quality (cross-section average SMD) versus atomizing air flow for SwRI 1.4-mm exit hole diameter, internal-mix, air-assist injector spraying methanol for 4-ms pulse width, 50-ms period (same as Figure 7, but for 1.4-mm hole diameter).

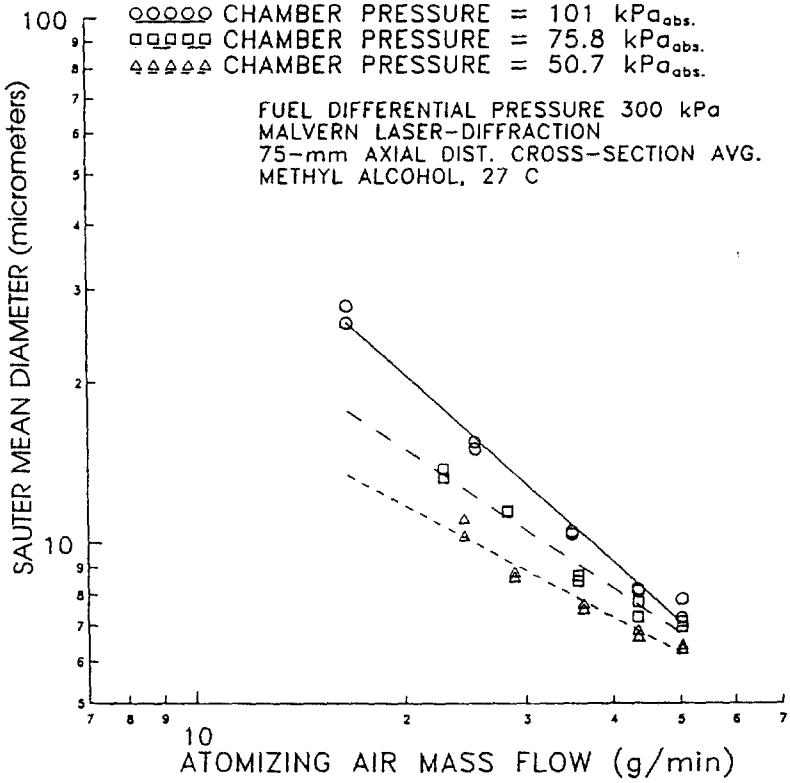

Figure 12. Atomization quality (cross-section average SMD) versus atomizing air flow for SwRI 1.4-mm exit hole diameter, internal-mix, air-assist injector spraying methanol for 10-ms pulse width, 50-ms period (same as Figure 8, but for 1.4-mm hole diameter).

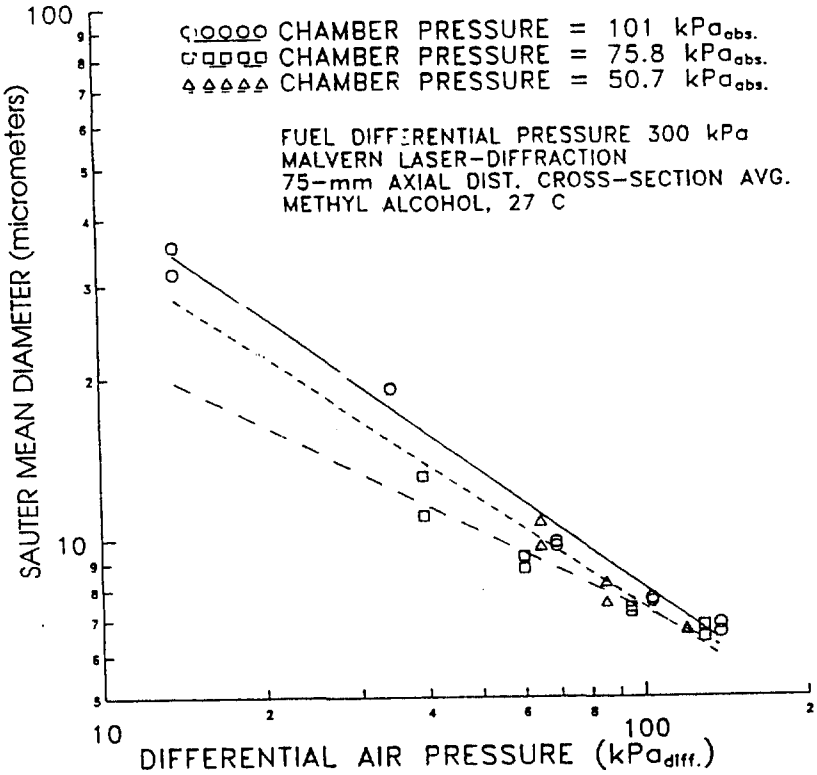

Figure 13. Atomization quality (cross-section average SMD) versus differential air pressure for SwRI 2.0-mm exit hole diameter, internal-mix, air-assist injector spraying methanol for 4-ms pulse width, 50-ms period (same as Figures 5 and 9, but 2.0-mm hole diameter).

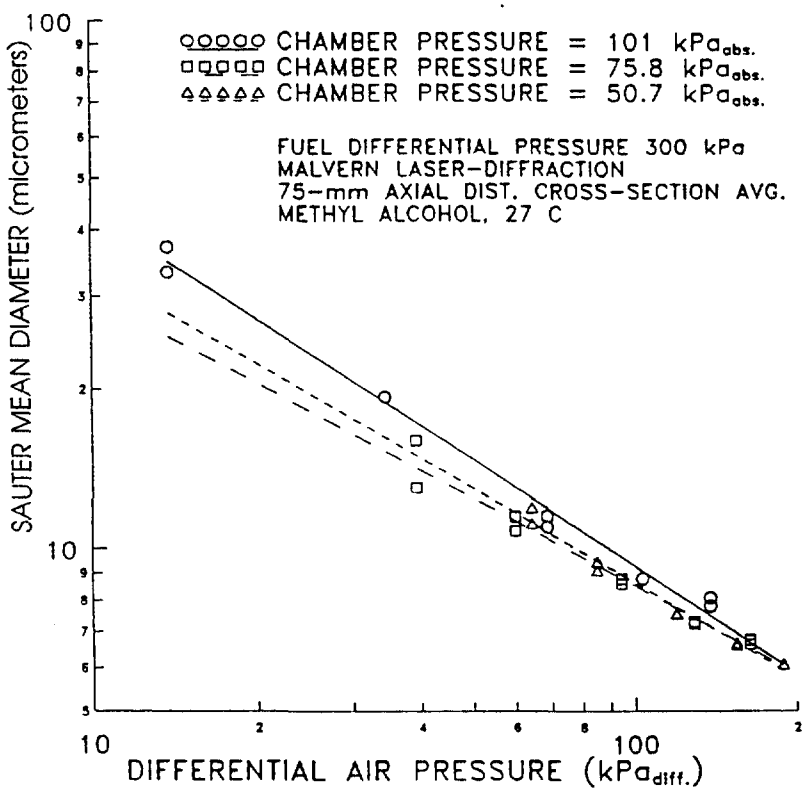

Figure 14. Atomization quality (cross-section average SMD) versus differential air pressure for SwRI 2.0-mm exit hole diameter, internal-mix, air-assist injector spraying methanol for 10-ms pulse width, 50-ms period (same as Figures 6 and 10, but 2.0-mm hole diameter).

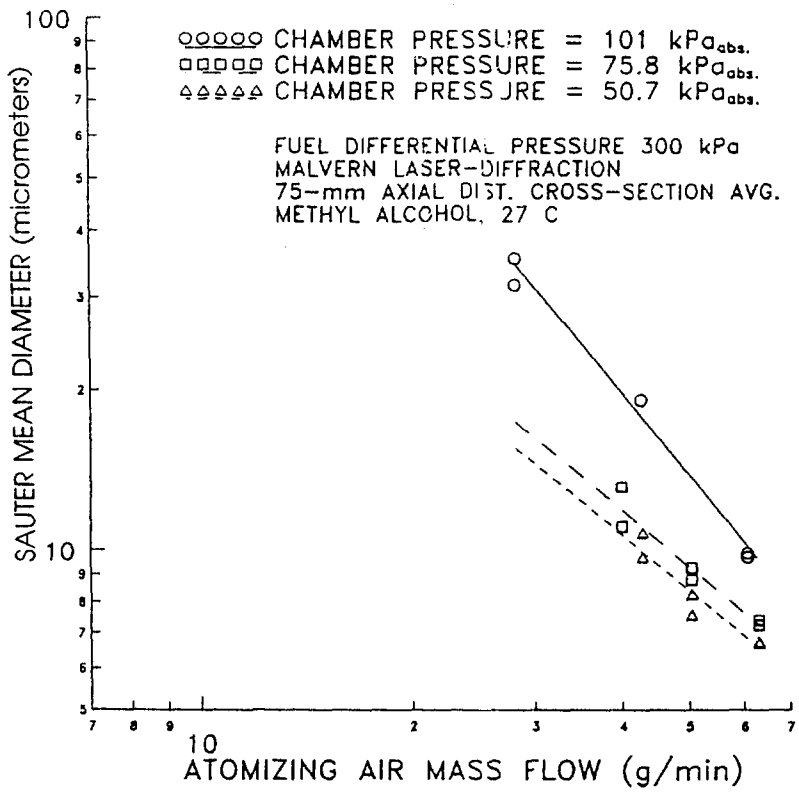

Figure 15. Atomization quality (cross-section average SMD) versus atomizing air flow for SwRI 2.0-mm exit hole diameter, internal-mix, air-assist injector spraying methanol for 4-ms pulse width, 50-ms period (same as Figures 7 and 11, but for 2.0-mm hole diameter).

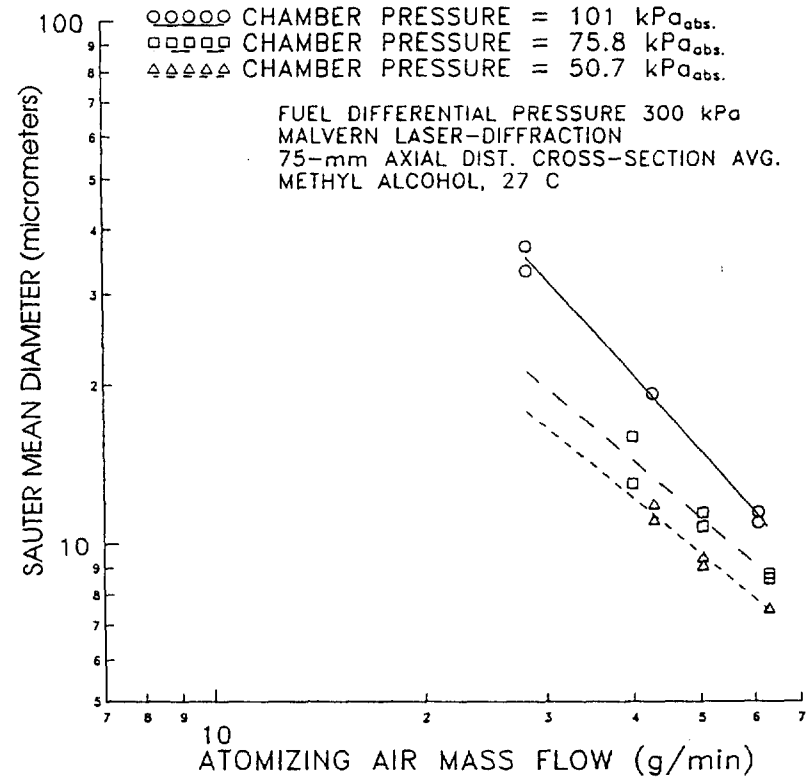

Figure 16. Atomization quality (cross-section average SMD) versus atomizing air flow for SwRI 2.0-mm exit hole diameter, internal-mix, air-assist injector spraying methanol for 10-ms pulse width, 50-ms period (same as Figures 8 and 12, but for 2.0-mm hole diameter).

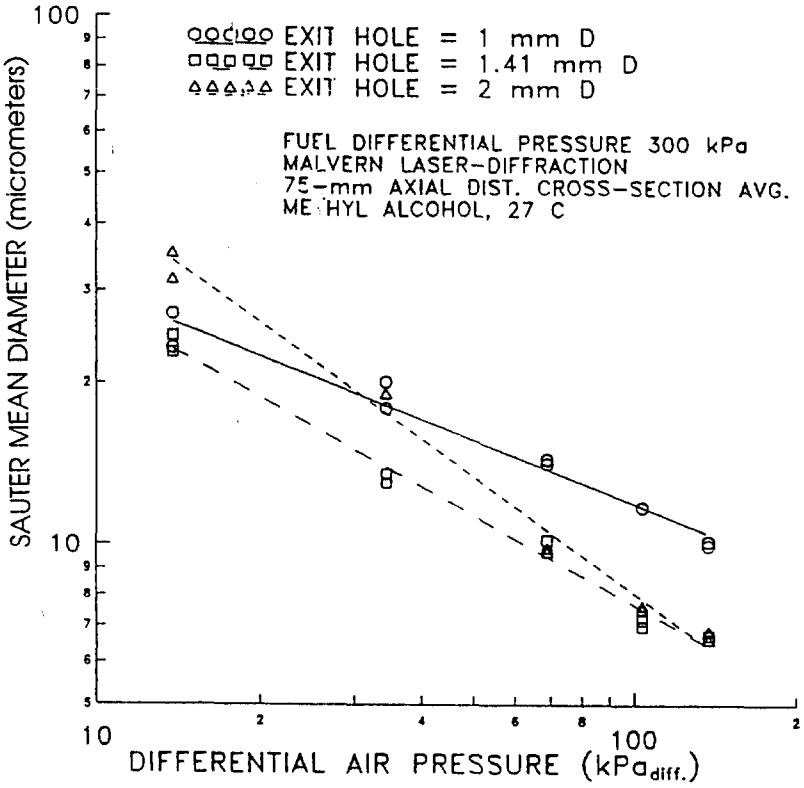

Figure 17. Comparison of atomization quality (SMDs) versus differential air pressure for three internal-mix, air-assist injectors with 1.0-mm, 1.4-mm, and 2-mm exit hole diameters, 4-ms pulse width, spraying into chamber at 101 $kPa_{absolute}$.

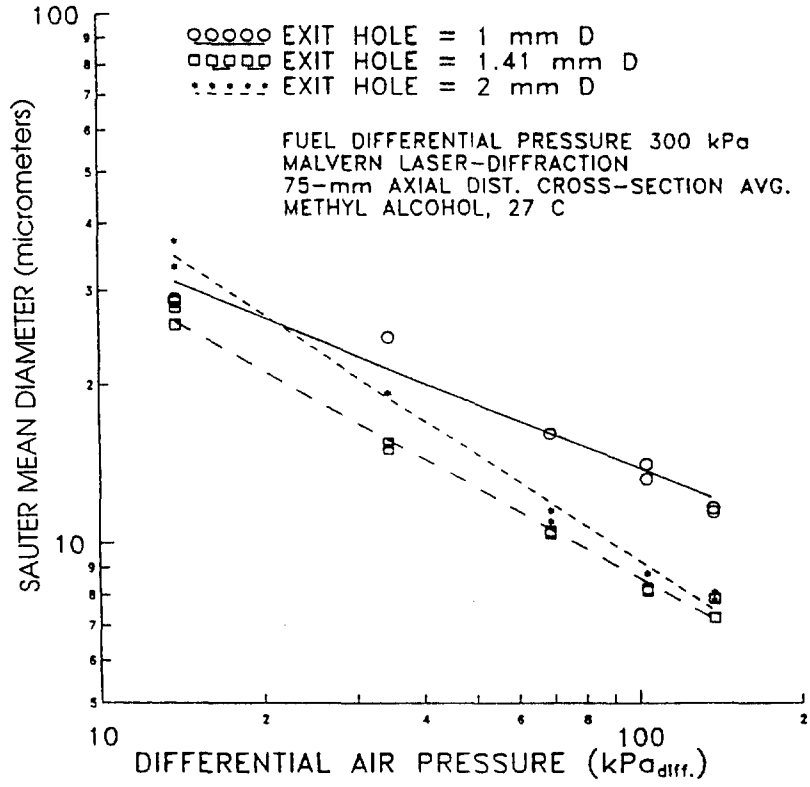

Figure 18. Comparison of atomization quality (SMDs) versus differential air pressure for three internal-mix, air-assist injectors with 1.0-mm, 1.4-mm, and 2-mm exit hole diameters, 10-ms pulse width, spraying into chamber at 101 $kPa_{absolute}$.

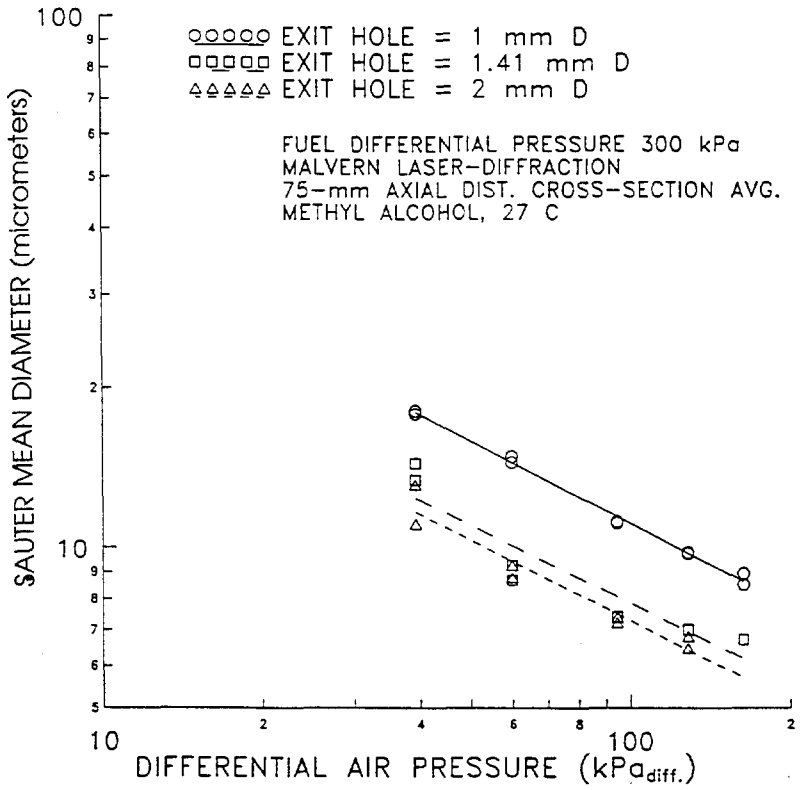

Figure 19. Comparison of atomization quality (SMDs) versus differential air pressure for three internal-mix, air-assist injectors with 1.0-mm, 1.4-mm, and 2-mm exit hole diameters, 4-ms pulse width, spraying into chamber at 75.8 $kPa_{absolute}$.

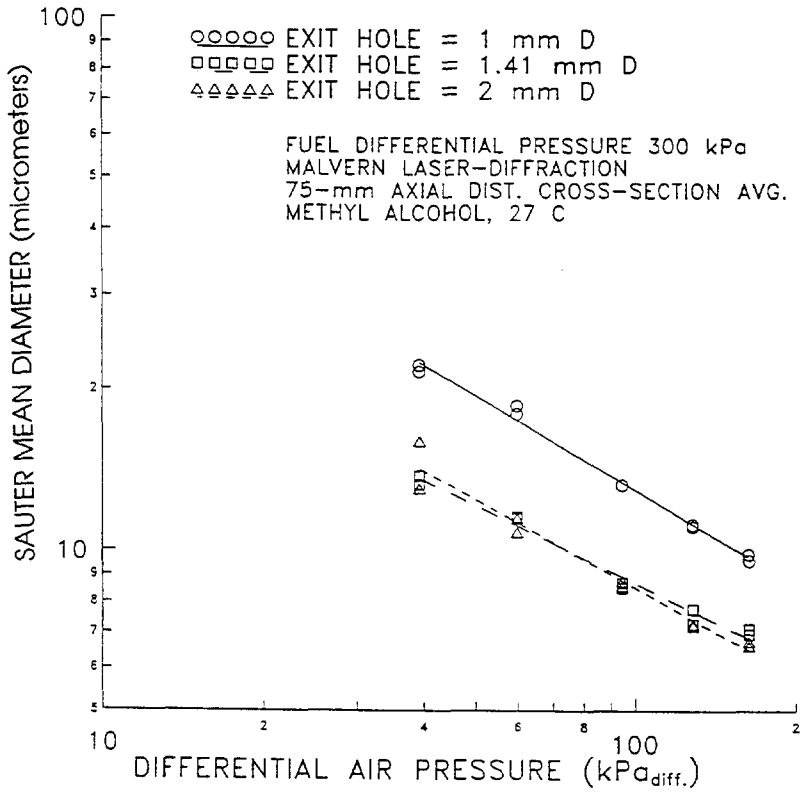

Figure 20. Comparison of atomization quality (SMDs) versus differential air pressure for three internal-mix, air-assist injectors with 1.0-mm, 1.4-mm, and 2-mm exit hole diameters, 10-ms pulse width, spraying into chamber at 75.8 $kPa_{absolute}$.

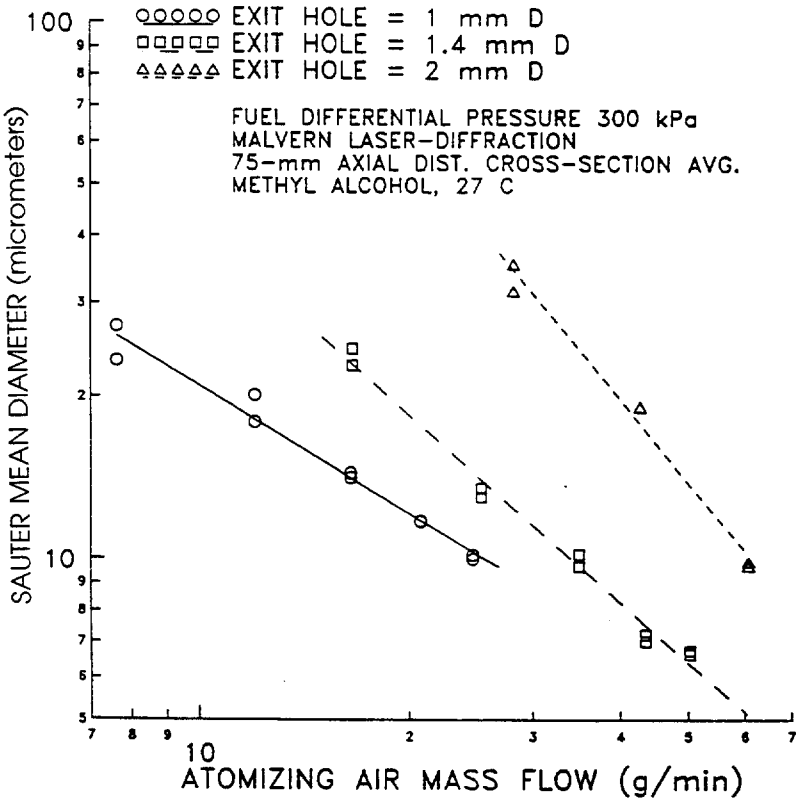

Figure 21. Comparison of atomization quality (SMDs) versus atomizing air-mass flow rate for three internal-mix, air-assist injectors with 1.0-mm, 1.4-mm, and 2-mm exit hole diameters, 4-ms pulse width, spraying into chamber at 101 $kPa_{absolute}$.

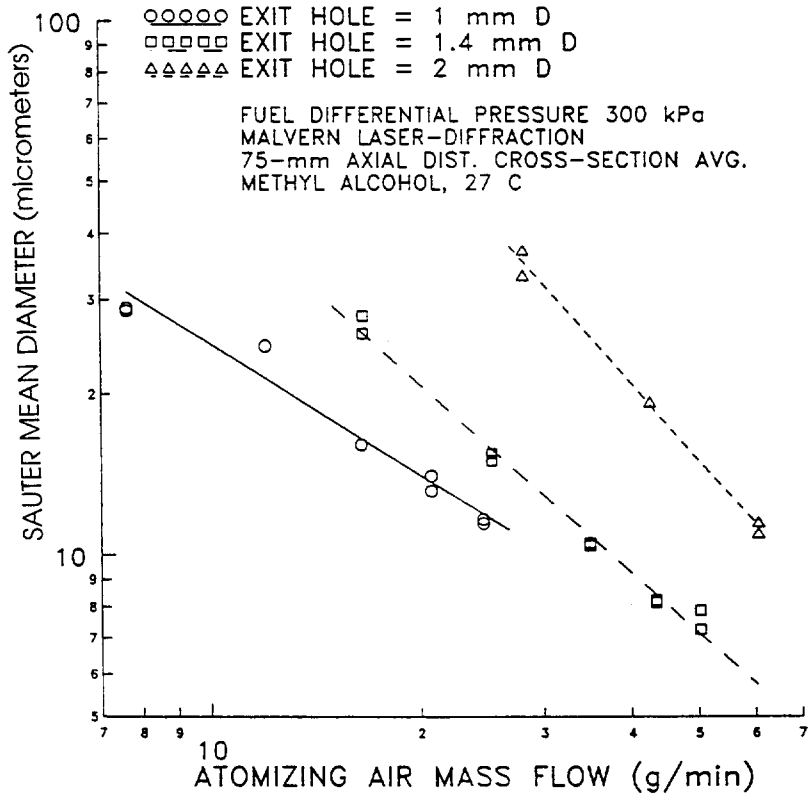

Figure 22. Comparison of atomization quality (SMDs) versus atomizing air-mass flow rate for three internal-mix, air-assist injectors with 1.0-mm, 1.4-mm, and 2-mm exit hole diameters, 10-ms pulse width, spraying into chamber at 101 $kPa_{absolute}$.

The air-flow requirements for the 1.4-mm diameter hole are only slightly greater than for the 1-mm diameter hole, but the atomization quality for a given differential pressure is much better for the 1.4-mm hole. The 2-mm diameter hole requires much more air than the 1.4-mm hole, but the atomization for a given differential air pressure at high air pressures is not much better than for the 1.4-mm hole. Therefore, the 1.4-mm hole appears to be about the optimum size for a methanol-fueled, air-assist injector over the range of pulse widths tested.

The goal of a 10-μm SMD is achieved with the 1.4-mm hole injector. It is possible to estimate the performance of this injector in engine cold-start applications. First, it is necessary to estimate the initial drop sizes at the injector because by the time the spray reaches the measurement location 75 mm from the injector tip, many of the small drops have already evaporated. The TESS computer model was used to estimate that, if the measured spray characteristics at 75 mm were an SMD of 7.6 μm and a Rosin-Rammler N (distribution width parameter) value of 1.74, then the spray characteristics at the injector tip were about an SMD of 4.5 μm and an N of 1.38. These characteristics can be used to estimate how the spray will perform in attempting to flow past the intake valve in a spark-ignition engine at a temperature of -29°C (-20°F).

Figure 23(a) shows the geometry of the air turning about 45° to flow past the intake valve and the liquid drops attempting to follow the airstream. The simplified geometry used for the TESS calculations is shown in Figure 23(b). Figure 24(a) shows the computed trajectories for the fine-spray injector when the spray reaches the intake valve. For this simulation, 82% of the spray turned and followed the airstream into the cylinder and another 11% evaporated, also making it into the cylinder. However, initially, the fuel spray is actually distributed more randomly than shown in the simulation, so a somewhat larger fraction of the spray collides with the intake valve. The important point is that a significant fraction of the original spray from the injector can be injected past the intake valve and into the cylinder without being prevaporized first.

Consider now the trajectories of drops from a conventional port injector compared with drops from the fine-spray, air-assist injector. For the conventional pintle port injectors, the SMD measured by laser-diffraction for a 10-ms pulse width was about 136 μm (number-density-weighted [NDW] sample format). (See Appendix A for a discussion of the effects of sampling format on drop-size measurements.) Using the TESS code, the original spray at the injector was determined to be about 200 μm, with a Rosin-Rammler N parameter of 2.4. Given the spray characteristics at the intake valve 130 mm downstream of the injector, spraying into air at -29°C (-20°F) and moving at 2.8 m/s, the TESS code predicted that the spray would have an SMD of about 204 μm (number-flux-weighted [NFW] average) and the original drop velocities of 16 m/s would decrease to about 11 m/s. These drop sizes and velocities are then used as input for a calculation of the spray trajectories past the intake valve, such as is illustrated in Figure 23(b). Results for the conventional pintle injector are shown in Figure 24(b). Essentially all the spray impacts the back of the intake valve, and none of the drops go directly into the cylinder. Thus, the fuel must prevaporize or travel as a liquid stream along the port walls or the intake valve to get into the cylinder. This introduces the time delays that necessitate fuel enrichment at low-temperature cold-starting and for accelerations.

It is already known from direct in-cylinder injection engine tests (Siewert and Groff 1987) that if the spray can make it into the cylinder, it can be ignited by direct-spark vaporization of the liquid and will then heat the resulting vapor-air mixture to combustible conditions (Jorgensen 1988). This is true even at temperatures of -29°C where it is not possible to prevaporize a combustible mixture of methanol. However, the approach described here of using port-fuel injectors is far simpler and more cost-effective than direct in-cylinder injection of the fuel.

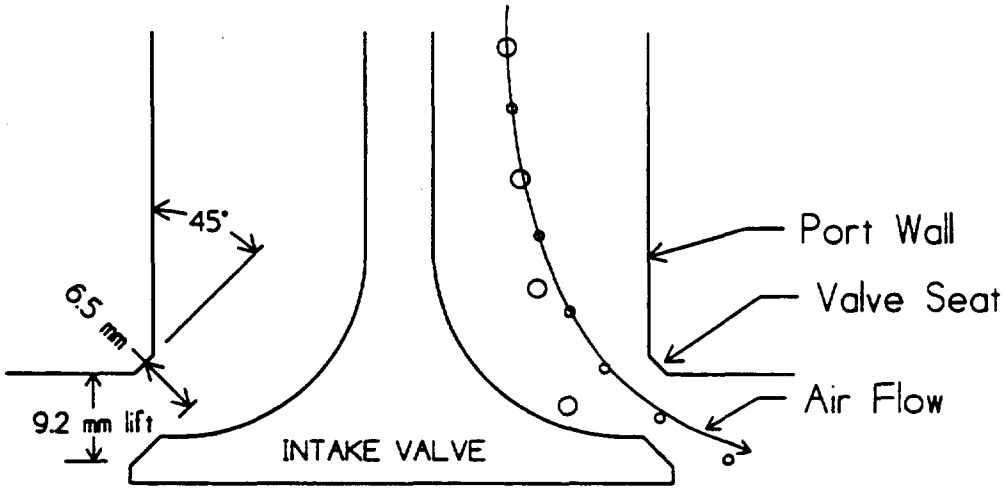

Figure 23(a). Flow of air and fuel spray past intake valve.

Note: Typical dimensions for a 0.5-L per cylinder engine are 30-mm port bore and 9-mm maximum valve lift. The air must turn about 45° in flowing past the valve, and the fuel drops will tend to separate out and strike the valve, with larger drops having greater centrifugal force than smaller drops that tend to follow the air stream.

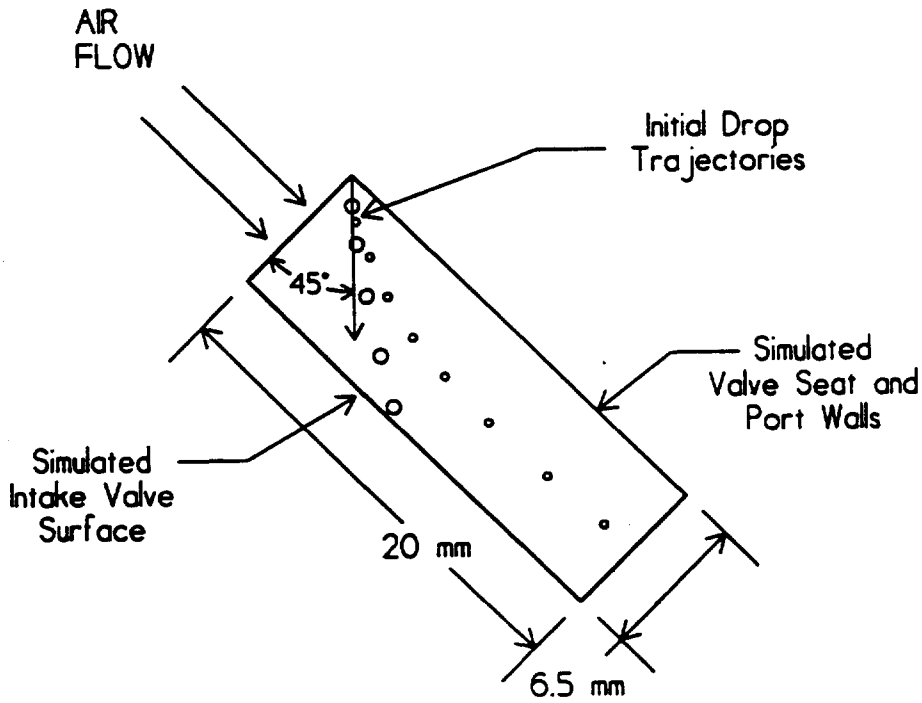

Figure 23(b). Simulation of the flow past the intake valve including 45° turn of air flow relative to the flow in the port.

Note: Dimensions are 6.5-mm height and 20-mm length.

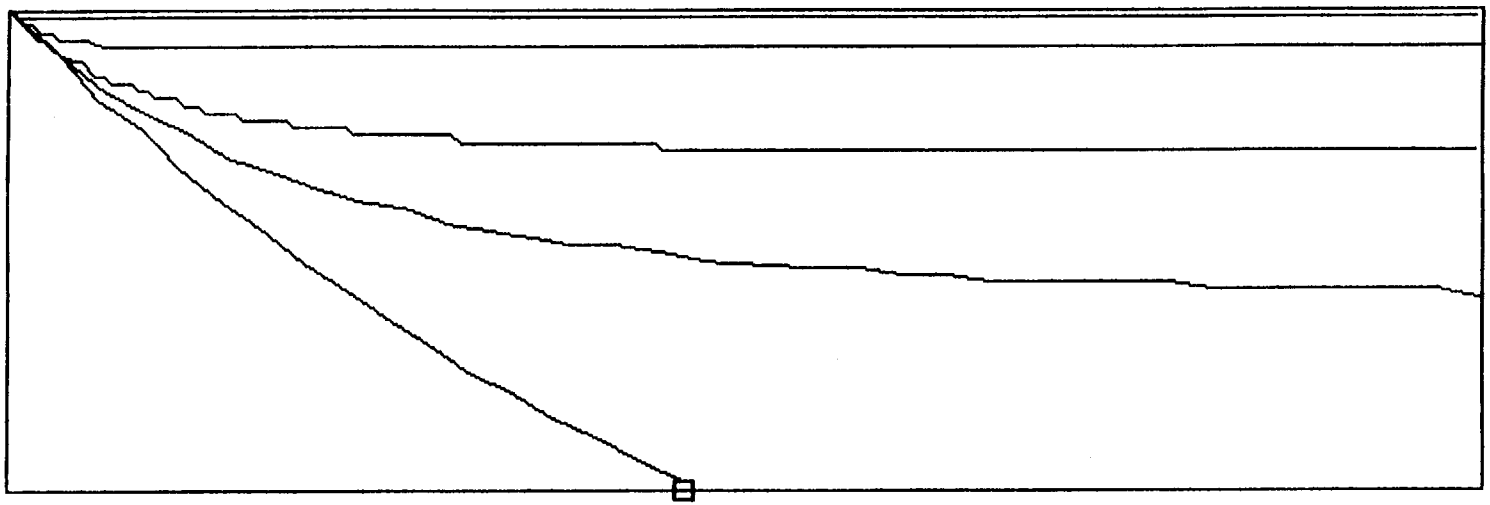

```
Trajectories shown for drop sizes (microns) =    2.    5.   10.   15.   30.
At an Axial Distance =     20.0 mm     or     .787 in.
Percentage of Liquid Evaporated =                  10.9 %
Percentage of Liquid on Wall =                      6.9 %
Percentage of Liquid as a Liquid in the Air =      82.2 %

Drop Size Dist.  R-R Xbar (um)   R-R N      SMD (um)  Dv0.5 (um)   Corr.Coef.
Number Flux Wt.       14.6         1.55        5.8        11.5         .998
Number Density Wt.    14.7         1.54        5.8        11.6         .998
Axial Air Velocity =  10.000 m/s,  Radial =     .000 m/s,  Air Temp =  -29.0 C
Steady-State Wet-Bulb Drop Temp = -33.8 C
    *** Computations complete. Press Return (Enter) to exit screen. ***
```

Figure 24(a). **Computed drop trajectories for fine-spray injector flow past intake valve (6.5-mm by 20-mm section) for drop sizes of 2 μm (at top), 5 μm, 10 μm, 15 μm, and 30 μm (at bottom).**

Note: Represents smallest 20% by volume segment of spray to largest 20% for methanol spray with initial spray characteristics at injector tip of SMD = 4.5 μm and Rosin-Rammler N parameter of 1.38, drop velocity at intake valve of 13 m/s, and air velocity (due to injector air jet) of 10 m/s at intake valve.

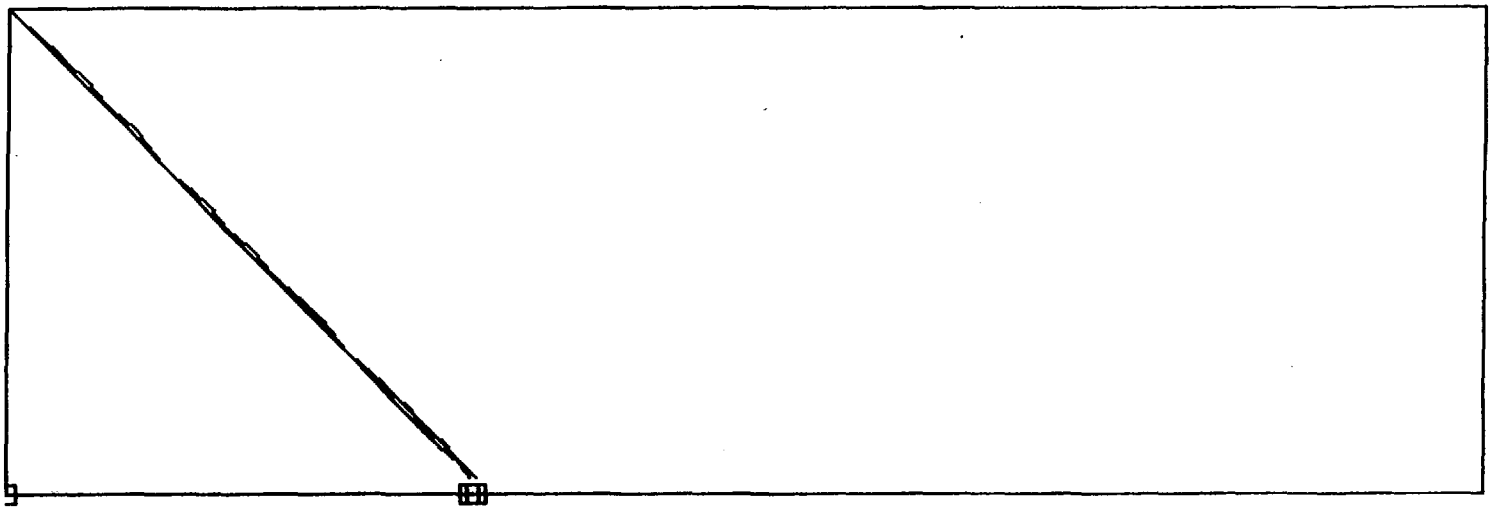

```
Trajectories shown for drop sizes (microns) =  100.  200.  300.  300.  400.
At an Axial Distance =     10.0 mm     or    .394 in.
Percentage of Liquid Evaporated =                  .0 %
Percentage of Liquid on Wall =                   99.6 %
Percentage of Liquid as a Liquid in the Air =      .4 %

Drop Size Dist.  R-R Xbar (um)   R-R N      SMD (um)  Dv0.5 (um)   Corr.Coef.
Number Flux Wt.       28.5        2.59        19.6        24.8         .997
Number Density Wt.    26.5        2.60        18.2        23.0         .997
Axial Air Velocity =   3.000 m/s,  Radial =    .000 m/s,  Air Temp =  -29.0 C
Steady-State Wet-Bulb Drop Temp = -33.8 C
    *** Computations complete. Press Return (Enter) to exit screen. ***
```

Figure 24(b). **Computed drop trajectories for conventional pintle injector flow past intake valve (6.5-mm by 20-mm section) for drop sizes of 100 μm, 200 μm, 300 μm, 300 μm, and 400 μm.**

Note: *Represents the smallest 20% by volume segment of spray to largest 20% for methanol spray with initial spray characteristics at injector tip of SMD = 200 μm, Rosin-Rammler N parameter 2.4, drop velocity of 11 m/s at the intake valve, and air velocity of 3 m/s at the intake valve.*

Thus, fine-spray air-assist fuel injectors successfully met the criteria of producing SMDs less than 10 μm using air-pressure differentials of only 70 kPa (10 psid, d = differential). On another project, slight modifications were made to the injector design shown in Figure 3 with almost a factor-of-two reduction in drop sizes from those shown in this report. This modified injector design may be available for future engine tests with the alcohol fuels.

Computational Evaluation of Fine-Spray Fuel Injectors

The above experimental and computational work demonstrates that it is possible to construct fine-spray port-fuel injectors that can inject methanol fuel sprays directly from the injector, past the intake valve, and into the cylinder. Further, these injectors can be controlled using standard PWM electronics. It will be necessary to calibrate the engine for these injectors, reducing fuel enrichment for cold-starting and accelerations from that used with conventional injectors. What can we expect if fine-spray injectors are used with alcohol fuels for spraying onto an open intake valve? A computer analysis was performed to estimate the impact of fine-spray injectors on cold-starts at various air temperatures and on steady-state combustion performance.

Computational evaluation of the fine-spray injectors required the use of the TESS spray code, previously developed at SwRI, and an internal-combustion engine cycle-simulation code. The cycle-simulation code computes air temperatures and pressures during intake and compression cycles, burning rates during the combustion phases, unburned and burned gas compositions and temperatures, air and fueling rates, power produced, etc. This cycle simulation also can be used to predict nitrogen oxide (NO_x) formation, including the effects of exhaust gas recirculation (EGR) and residual gases, humidity, intake air temperature, etc. By combining the TESS code with the cycle-simulation code, it was possible to use the cycle simulation to estimate the instantaneous air temperatures and pressures and to include these effects on the fuel spray evaporation rate.

A detailed mathematical development of the TESS code is provided in Appendix A. It should be noted that the TESS code was developed prior to this contract and is not the property of DOE or NREL. However, for completeness, the operation of TESS is fully documented in the appendix. The cycle simulation is under development for a diesel engine consortium, and a more complete description of its operation is not available at this time. However, most of the features pertinent to this project are described above.

Most of the computational work concerned cold-start tests. The engine chosen was a 3.0-L Ford engine used in the Taurus, currently the largest selling vehicle in the United States. Some of the engine details are provided in Table 1. The boiling point and latent heat of vaporization for each fuel are shown in Table 2.

Cold-Start Tests

Cold-start tests assumed starting air and engine coolant temperatures of -25°C (-13°F), 0°C (32°F), and 25°C (77°F). Some parametric studies were performed for the 0°C condition. Cranking speeds were assumed to be 120 rpm at -25°C, 170 rpm at 0°C, and 250 rpm at 25°C. The computations were for these cranking conditions, and assumed intake and exhaust pressures of 100 $kPa_{absolute}$ (14.6 psia). Cranking is of particular interest for ultra-low emissions vehicles (ULEV) because a few misfires or lack of burns during cranking produce enough unburned fuel to fail the test. All calculations assumed that the fuel enters the cylinder at 90 crank angle degrees (CAD) from top-dead-center (TDC) on the intake stroke, or when the piston is halfway down on the intake stroke. (TDC firing is 360 CAD.) The spray was assumed to enter the cylinder as a fine liquid spray with an SMD of 10 μm and a Rosin-Rammler distribution width parameter N (see Appendix A) of 1.5, with no prevaporization. For these fine sprays, the fuel quickly

Table 1. Specifications of Ford Taurus 3.0-L Engine

Bore	89 mm
Stroke	80 mm
Rod Length	140 mm
Compression Ratio	9.3
Cylinders	6
Cycles	4
Swirl No.	0.3
Intake Valve Opening	698.5 CAD
Intake Valve Closing	252.5 CAD
Exhaust Valve Opening	469.5 CAD
Exhaust Valve Closing	23.5 CAD

Table 2. Fuel Properties

Fuel	Boiling Point (°C)	Latent Heat of Vaporization (kJ/kg)	Molecular Weight	Air/Fuel, Stoichiometric (Dry Air)
n-Heptane	98.4	317.8	100.2	15.21
California Phase II Gasoline	96.	350.		≈14.7
Ethanol	78.3	962.6	46.1	9.01
Methanol	64.7	1120.6	32.0	6.48

evaporated and reached equilibrium with the surroundings, cooling the air and saturating it with fuel vapor. This stopped further evaporation, especially for the alcohol fuels. Therefore, including the prevaporization in the port did not change the in-cylinder results.

Figures 25-27 show the evaporated fuel fraction during cranking for n-heptane, representing the mid-point of gasoline, neat ethanol, and neat methanol for air and engine temperatures of 25°C (77°F), 0°C (32°F), and -25°C (-13°F), respectively. Note that for the mid-point of gasoline simulated by n-heptane, evaporation is complete or close to complete before TDC, while in no case are ethanol or methanol completely evaporated by TDC. Because the amount of fuel injected was for a stoichiometric mixture in the cylinder, the n-heptane prevaporizes in the cylinder to a flammable vapor-air mixture for all cases.

The lean limit for combustion is about 60% of stoichiometry, hence the ethanol prevaporizes in the cylinder to above the lean limit for these conditions. However, once the engine begins firing and the speed increases, there is probably not sufficient time for prevaporization above the flammability limit. The

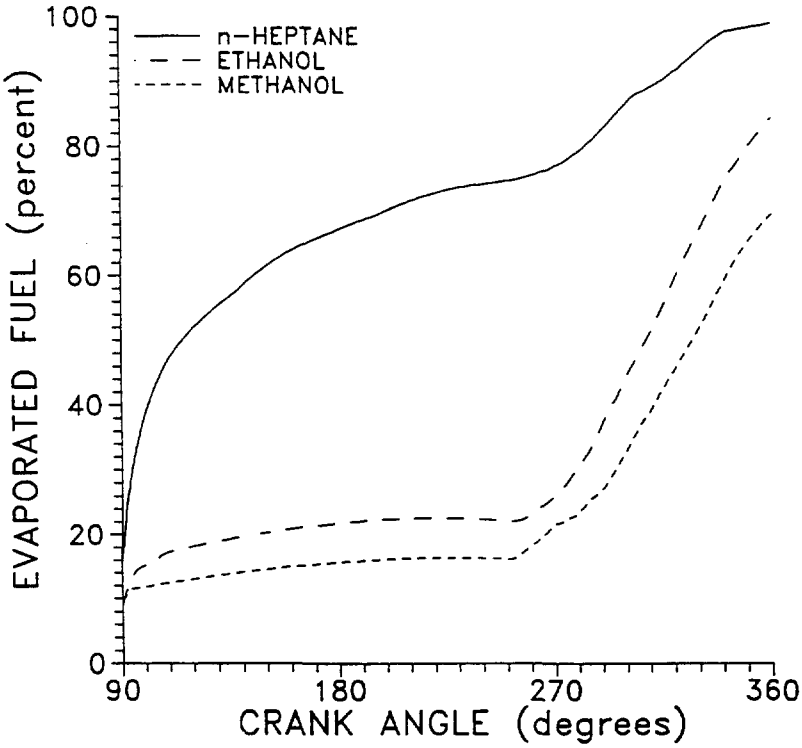

Figure 25. Comparison of in-cylinder evaporation of n-heptane (representing mid-point of gasoline), ethanol, and methanol, in Ford 3.0-L V6, 25°C air and engine temperature, 250 rpm, fuel spray SMD = 10 μm, Φ = 1.0, compression ratio = 9.3.

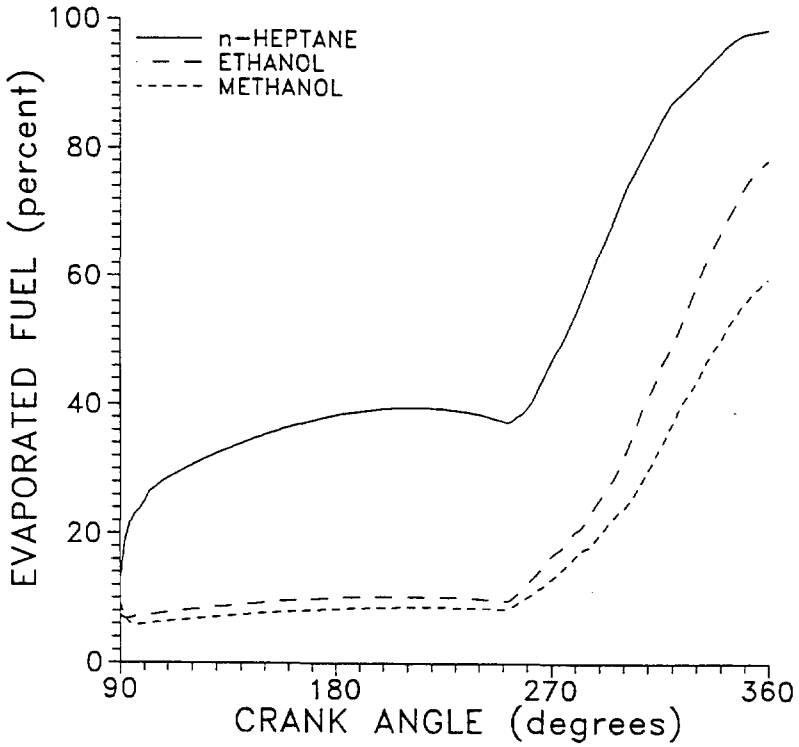

Figure 26. Same as Figure 25, but at 0°C air and engine temperatures and 170 rpm.

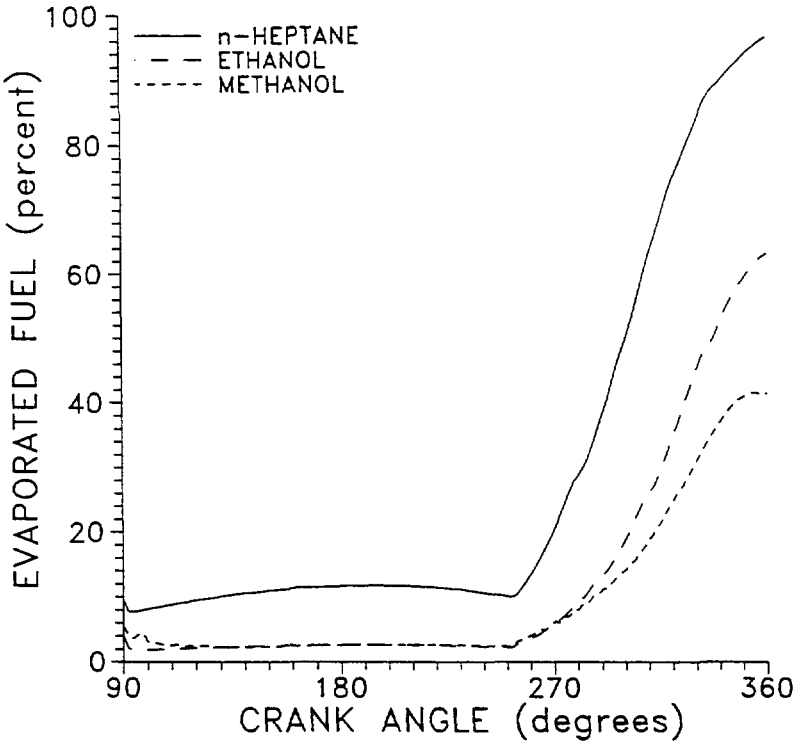

Figure 27. Same as Figures 25 and 26, but at -25°C air and engine temperatures and 120 rpm.

methanol evaporates more slowly than the ethanol, and below 0°C the compressional heating is not sufficient to produce a flammable mixture.

Thus, for the neat alcohol fuels, prevaporization of a flammable vapor-air mixture is difficult or impossible, even if the spray can be injected directly into the cylinder. This contrasts with the fact that Siewert and Groff (1987) demonstrated successful starts with neat methanol (M100) at -29°C (-20°F) using a direct-injected engine. The compression ratio of that engine was 13:1 rather than the 9.3:1 for this 3-L engine, but the calculations of compression heating for that engine again show that a combustible prevaporized mixture cannot be generated in the short time available for a direct-injected fuel spray. Therefore, Jorgensen (1988) postulated that combustion occurred when the spark energy was used to both vaporize the liquid fuel and then heat the fuel-air mixture to combustion temperatures. This is the same mechanism used to start gas-turbine engines that use very nonvolatile fuels at low temperatures. This is feasible if the fuel spray can be maintained in the air rather than being deposited on the walls of the combustion chamber. It is more difficult to keep the port-injected spray off the walls because it must remain suspended through both the intake and compression strokes, while the direct-injected spray must stay suspended for only 10 or 20 CAD.

The alcohol fuels evaporate more slowly than gasoline (n-heptane in this simulation) because of their high heat of vaporization, as shown in Table 2. The boiling points of the alcohols are actually lower than the n-heptane, as shown in Table 2. The fuel evaporation rapidly cools the air for these fine-spray injectors, as shown in Figure 28 for 25°C and in Figure 29 for 0°C. Methanol cools the air the most, followed by ethanol, and then n-heptane.

The TESS/CYCLE model also can be used to evaluate hydrocarbon levels expected in-cylinder; for gasoline or heptane, these values may be compared with measurements by a fast-response hydrocarbon analyzer. Figure 30 shows predicted hydrocarbon levels for the 0°C case expressed as parts per million

of carbon (ppmC). Stoichiometric mixtures are about 127,000 ppmC, and lean limits are about 60% of that value.

Some interesting differences exist in the evaporation-rate controlling mechanisms for these fine sprays for the different fuels. For n-heptane, even these fine sprays are limited in evaporation rate by the mass transfer rate of the fuel from the drop surface. This is illustrated in Figure 31, which shows the saturation fuel partial pressure at the drop surface compared with the free-stream fuel partial pressure for the 0°C cranking condition. The difference between these values is the driving force for evaporation at every crank angle. As soon as the fuel is injected at 90 CAD, the air cools and is saturated with fuel vapor, so there is very little driving force for evaporation between about 100 and 250 CAD. After 250 CAD, the air temperature rises due to compression heating, and the driving force for evaporation is large.

Contrast Figure 31 with Figures 32 and 33 for the same cranking condition using ethanol and methanol, respectively. For the ethanol spray shown in Figure 32, there is again saturation between about 100 and 250 CAD, but beyond 250 CAD the difference between the fuel vapor pressure at the surface of the drop (wet-bulb saturation pressure) and in the bulk cylinder gases is much less than for n-heptane; therefore, the driving force for evaporation is much less. For the methanol fuel shown in Figure 33, the driving force for evaporation is even smaller than for ethanol. Figure 33 shows that the evaporation of the methanol spray is not limited by mass transfer from the drops, but by the enthalpy (heat energy) available in the cylinder.

The wet-bulb saturation vapor pressure is lower for the alcohols than for n-heptane because the wet-bulb temperatures for the n-heptane are lower due to the larger latent heats of vaporization that cool both the

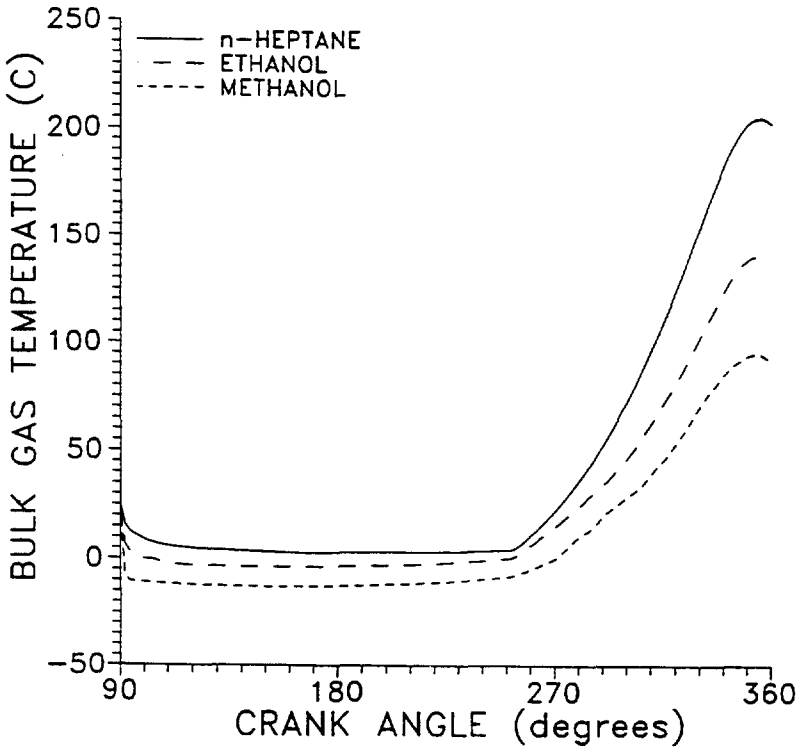

Figure 28. Bulk in-cylinder gas temperature for stoichiometric fuel sprays of n-heptane (representing gasoline), ethanol, and methanol for Ford 3.0-L V6, 25°C air and engine temperature, 250 rpm, fuel spray SMD = 10 μm, Φ = 1.0, compression ratio = 9.3.

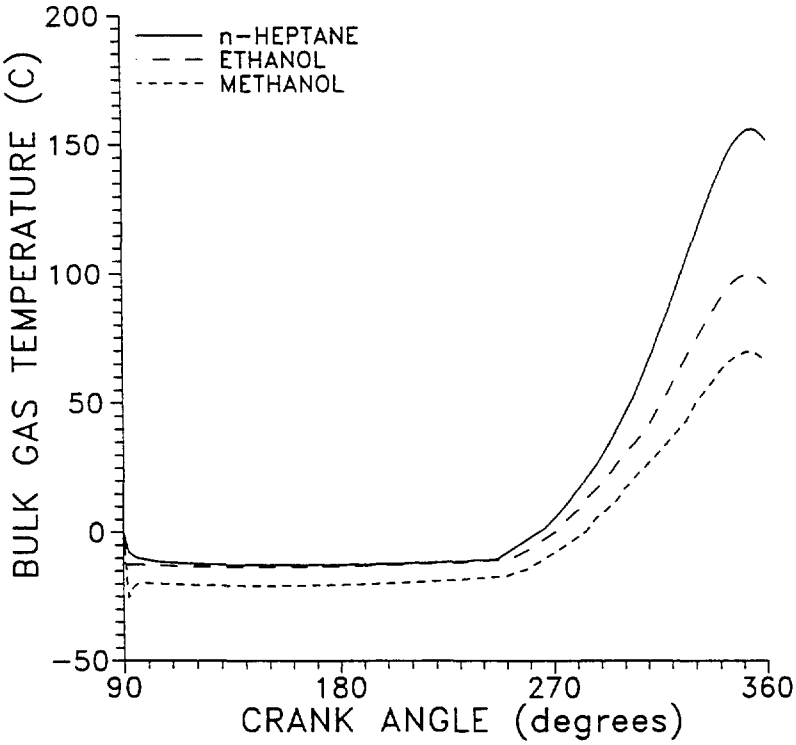

Figure 29. **Same as Figure 28, but at 0°C air and engine temperatures and 170 rpm.**

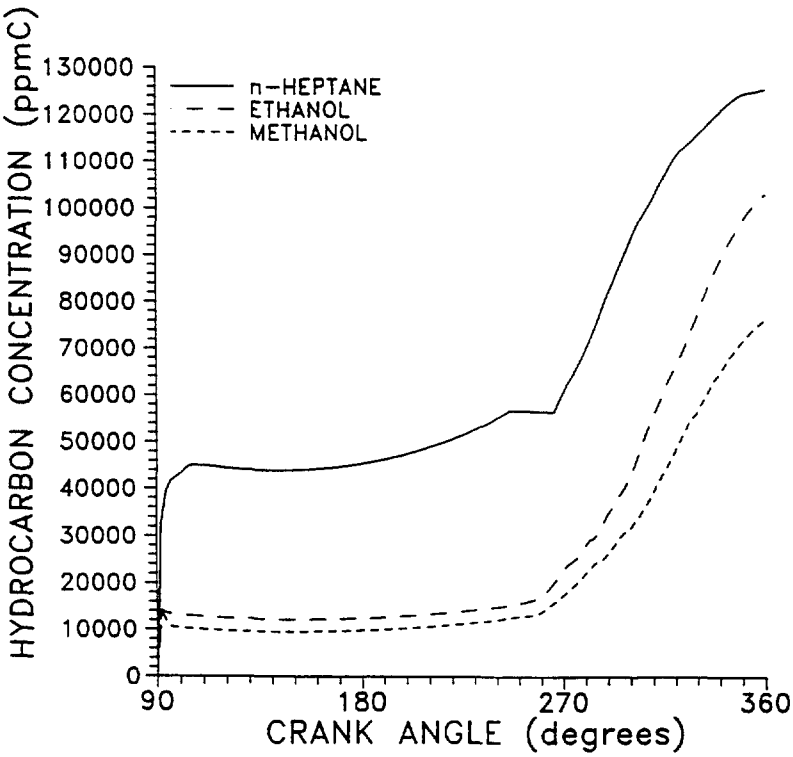

Figure 30. **In-cylinder fuel vapor concentration (in ppmC) comparing evaporation of n-heptane, ethanol, and methanol, for Ford 3.0-L V6, 0°C air and engine temperature, 170 rpm, fuel spray SMD = 10 μm, Φ = 1.0, compression ratio = 9.3.**

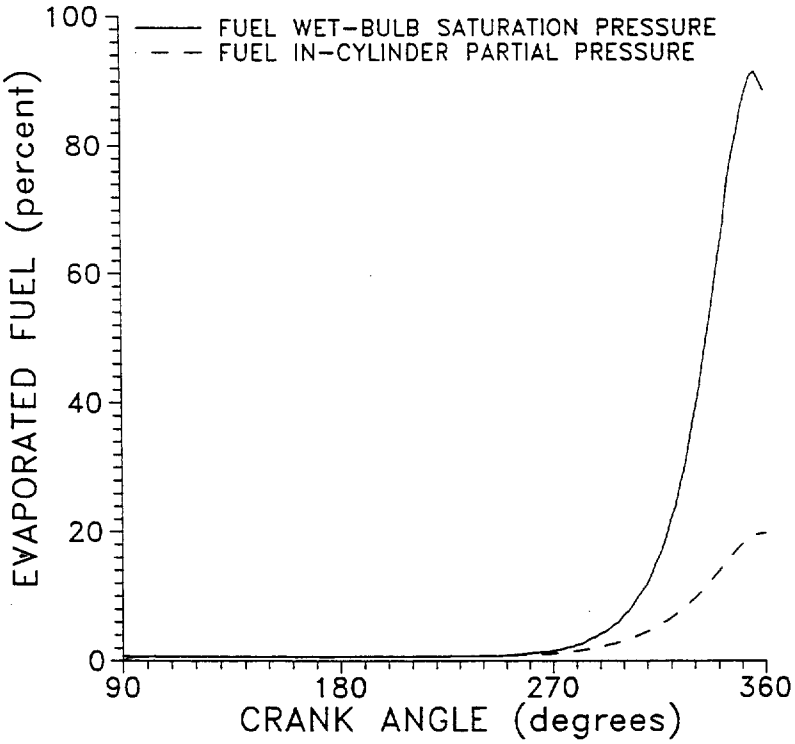

Figure 31. **Comparison of n-heptane fuel wet-bulb saturation pressure at surface of evaporating drop with bulk in-cylinder partial pressure; conditions for Ford 3.0-L V6, 0°C air and engine temperature, 170 rpm, fuel spray SMD = 10 μm, Φ = 1.0, compression ratio = 9.3. (Difference is driving force for evaporation.)**

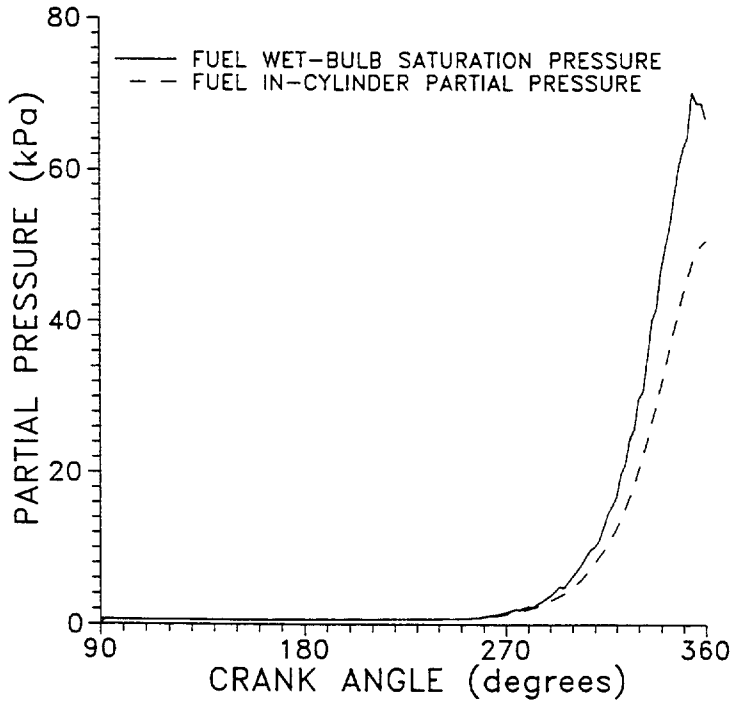

Figure 32. **Comparison of ethanol fuel wet-bulb saturation pressure at surface of evaporating drop with bulk in-cylinder partial pressure; conditions for Ford 3.0-L V6, 0°C air and engine temperature, 170 rpm, fuel spray SMD = 10 μm, Φ = 1.0, compression ratio = 9.3. (Difference is driving force for evaporation.)**

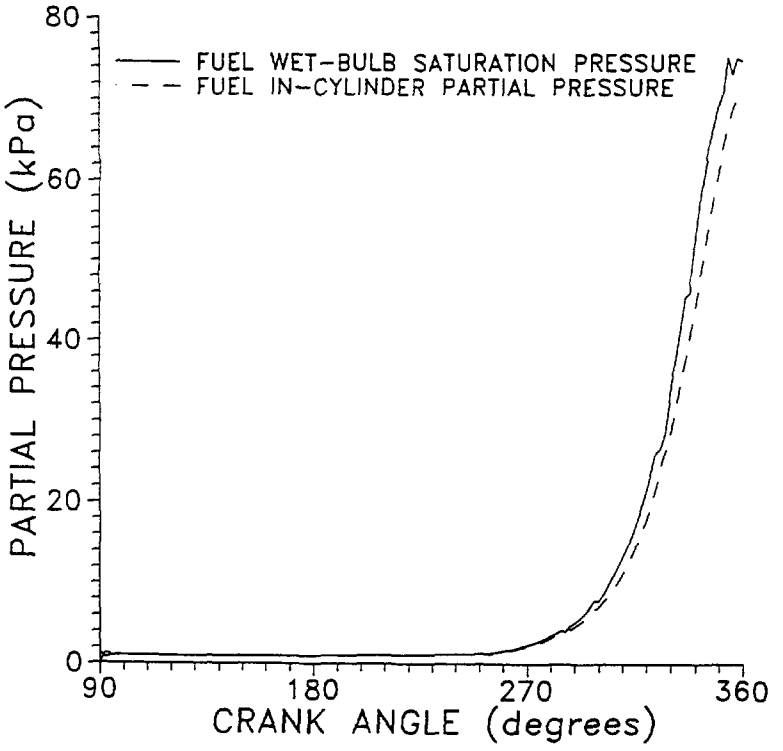

Figure 33. Comparison of methanol fuel wet-bulb saturation pressure at surface of evaporating drop with bulk in-cylinder partial pressure; conditions for Ford 3.0-L V6, 0°C air and engine temperature, 170 rpm, fuel spray SMD = 10 μm, Φ = 1.0, compression ratio = 9.3. (Difference is driving force for evaporation.)

liquid drops and the air. Even more significantly, the bulk in-cylinder vapor concentrations are much higher for the alcohols than for n-heptane for two reasons. First, when a given mass of the alcohol fuel makes the transition from liquid to vapor, it creates many more moles of gas because of the lighter molecular weights of the alcohols. Secondly, because of the lower air:fuel ratios for stoichiometric combustion of alcohols, a greater mass of the alcohol fuels must be injected, as shown in Table 2.

The differences shown in Figures 31-33 have some very important practical implications. First, for these very fine methanol sprays, evaporation at these conditions is not limited by mass transfer rates from the drops. Therefore, making the methanol spray finer than the 10 μm SMD used in the calculations will not enhance the amount of fuel evaporated. However, sprays with drop sizes larger than about 10 μm SMD will be limited by drop mass-transfer rates, and larger drop-size sprays will therefore evaporate more slowly. Another implication of these results is that enrichment of the fuel to help in cold-starting will be effective for n-heptane in raising the vaporized fuel concentration in the cylinder, while it is only slightly helpful for the ethanol, and not helpful for the methanol sprays.

To prove this last point, calculations at the 0°C condition were repeated with twice the stoichiometric amount of fuel injected, with predicted hydrocarbon concentrations as shown in Figures 34-36 for n-heptane, ethanol, and methanol, respectively. The concentration of n-heptane in-cylinder is greatly increased by the addition of more fuel. For ethanol, the extra fuel is only partially vaporized, and for methanol, there is no increase in the vaporized fuel concentration with fuel enrichment. Again, there is simply no thermal energy available in the methanol case to evaporate any more fuel. In practical applications, the methanol-fueled engine may be helped in cold-starting by enrichment because some fuel will be lost on the port walls and the combustion chamber walls. However, Figures 34-36 show that fuel enrichment for alcohols is not nearly as beneficial as for gasoline-fueled engines.

How can low-temperature cold-starts be achieved with the alcohol fuels if enrichment does not help in the in-cylinder evaporation? Hydrocarbon light-ends can be added, of course. Direct-spark vaporization and ignition is potentially attractive if the spray can be retained in the air. It is difficult to address the direct-spark vaporization beyond what has been presented here, and this approach needs to be examined with engine tests. Alcohol fuels have much higher octane numbers than gasoline, so higher compression ratios may be used, increasing the compression temperature. Interestingly, this results in only slight improvements in the amount of fuel vaporized, as shown in Figure 37. However, the increased compression ratio helps cycle efficiency considerably and should be employed for dedicated alcohol engines.

Steady-State Operation at Road-Load

The above discussion on computations addresses cold-starts. One set of calculations was also run at a road-load condition for the 3-L Ford Taurus engine of 2100 rpm, stoichiometric fuel-air ratio, intake manifold pressure of 40 $kPa_{absolute}$, exhaust pressure of 102 $kPa_{absolute}$, barometric pressure of 100 $kPa_{absolute}$, intake air temperature of 25°C, coolant temperature of 90°C, spark advance of 23°BTDC (before top-dead-center), which on n-heptane fuel is predicted to produce a brake mean effective pressure (BMEP) of 184 kPa (27 psi), and a power of 9.6 kW (12.9 HP). Although the engine is warm for these calculations, Figure 38 shows that the direct injection of fuel into the cylinder can lead to limited evaporation of the alcohol fuels because, compared with the cranking calculations, there is much less time available for evaporation. At the time of the spark (337 CAD), about 80% of the freshly injected n-heptane is evaporated, while about 50% of the ethanol and 45% of the methanol is evaporated. In an operating engine, a significant fraction of the fuel on a given cycle is fuel injected for previous cycles that

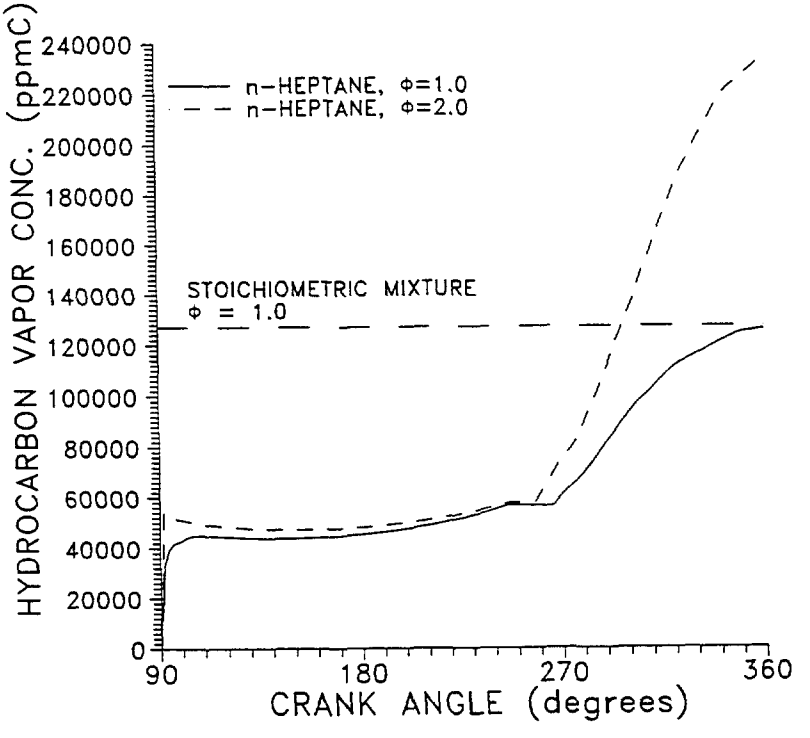

Figure 34. Effect of enrichment for n-heptane (simulating mid-point of gasoline) from Φ = 1.0 (stoichiometric) to Φ = 2.0 for n-heptane (simulating mid-point of gasoline) on fuel vapor in-cylinder during cranking for Ford 3.0-L V6, 0°C air and engine temperature, 170 rpm, fuel spray SMD = 10 μm, Φ = 1.0, compression ratio = 9.3.

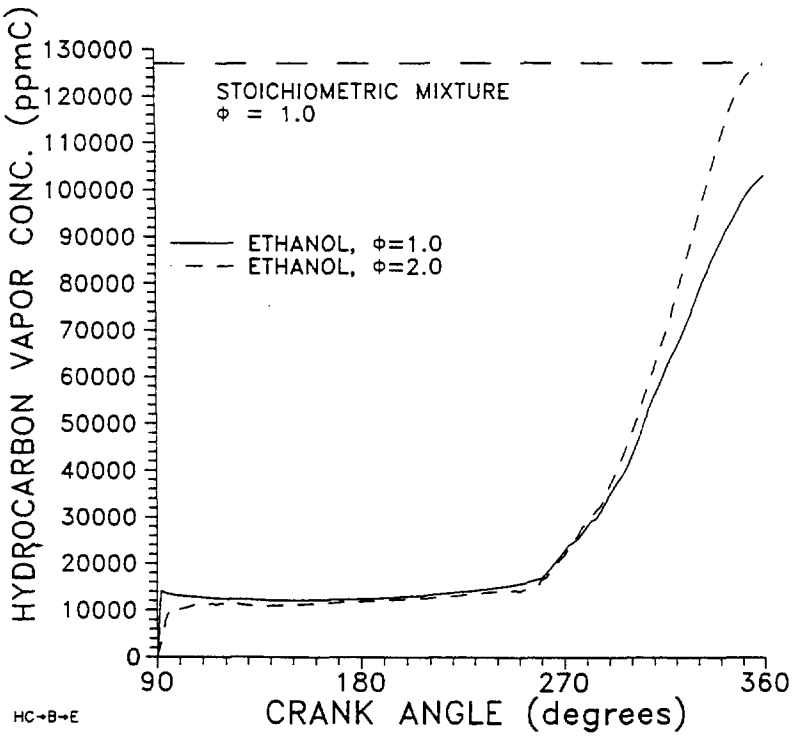

Figure 35. Effect of enrichment for ethanol (simulating mid-point of gasoline) from Φ = 1.0 (stoichiometric) to Φ = 2.0 for n-heptane (simulating mid-point of gasoline) on fuel vapor in-cylinder during cranking for Ford 3.0-L V6, 0°C air and engine temperature, 170 rpm, fuel spray SMD = 10 μm, Φ = 1.0, compression ratio = 9.3.

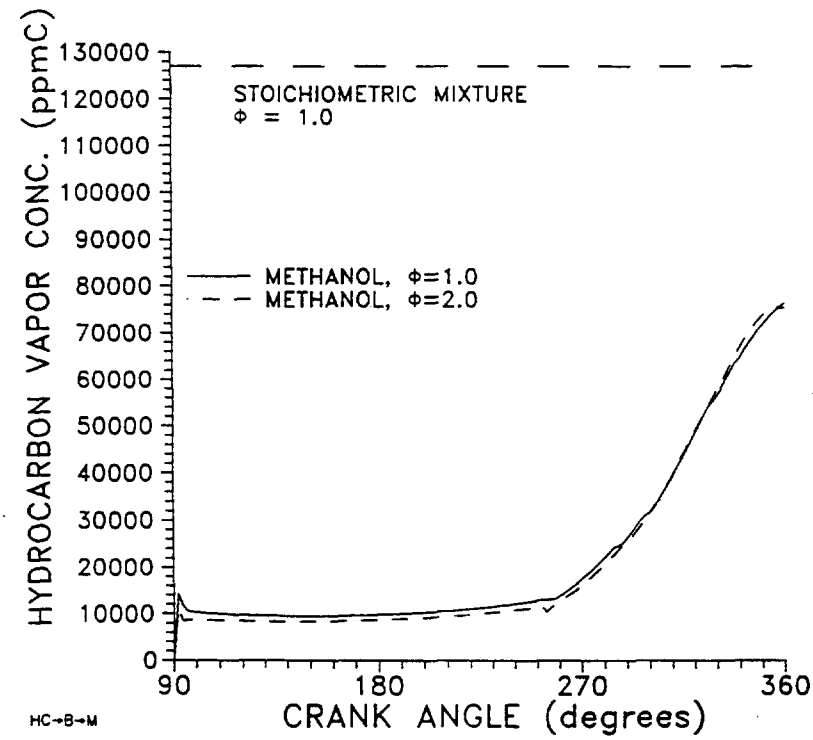

Figure 36. Effect of enrichment for methanol (simulating mid-point of gasoline) from Φ = 1.0 (stoichiometric) to Φ = 2.0 for n-heptane (simulating mid-point of gasoline) on fuel vapor in-cylinder during cranking for Ford 3.0-L V6, 0°C air and engine temperature, 170 rpm, fuel spray SMD = 10 μm, Φ = 1.0, compression ratio = 9.3.

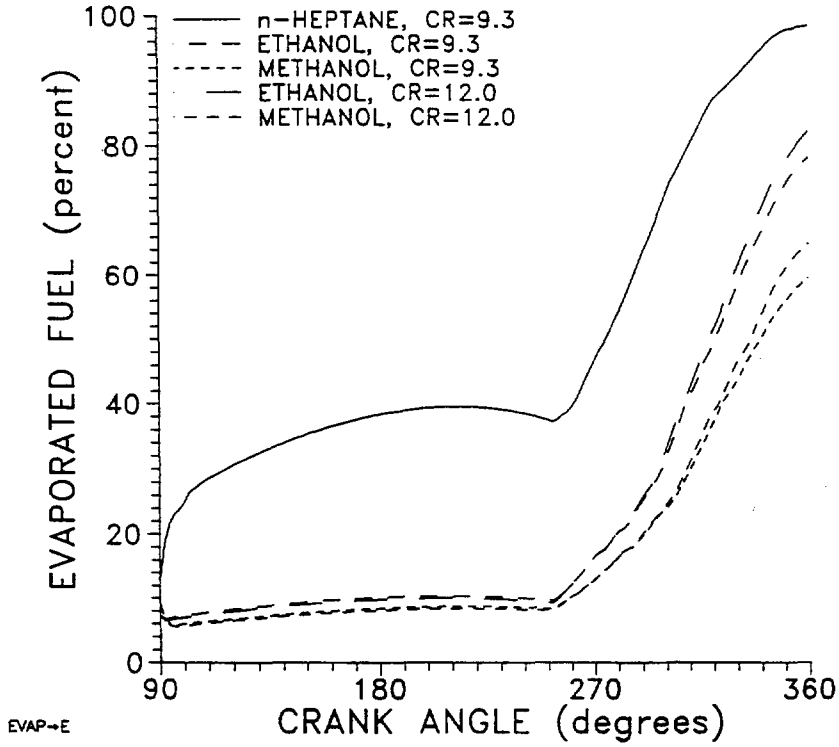

Figure 37. **Effect of increasing compression ratio for alcohol fuels on in-cylinder evaporation rates for n-heptane (representing gasoline), ethanol, and methanol during cranking for Ford 3.0-L V6, 0°C air and engine temperature, 170 rpm, fuel spray SMD = 10 μm, Φ = 1.0, compression ratio = 9.3 and 12.0.**

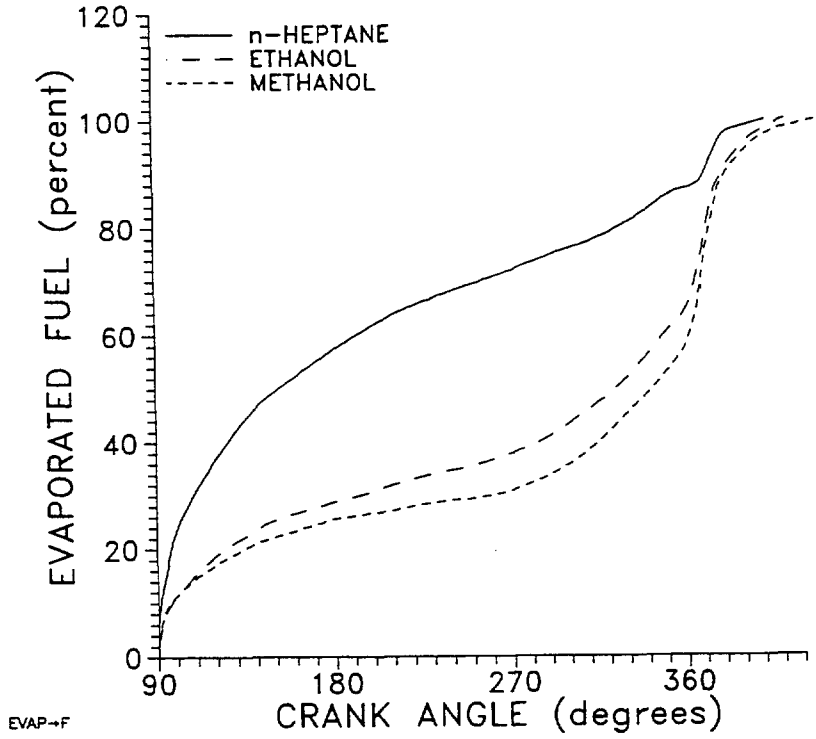

Figure 38. **Comparison of in-cylinder evaporation of n-heptane (representing mid-point of gasoline), ethanol, and methanol in Ford 3-L V6, 25°C air inlet, 90°C coolant, 2100 rpm, fuel spray SMD = 10 μm, Φ = 1.0, compression ratio = 9.3**

Table 3. Comparison of Fuel Effects on Predicted Power and Efficiency

Fuel	Compression Ratio	BMEP (kPa)	Power (kW)	Brake Thermal Efficiency (%)	Percent Improvement Relative to Heptane
n-Heptane	9.3	184	9.6	18.3	0.0
Ethanol (E100)	9.3	198	13.8	19.3	5.5
Methanol (M100)	9.3	208	14.6	20.0	9.3
Ethanol (E100)	12.0	243	17.0	22.7	24.0
Methanol (M100)	12.0	255	17.9	23.5	28.4

has been vaporized for a cycle length or longer in the intake system. Once the combustion begins, these calculations indicate that the fine sprays are completely vaporized. However, larger drops are predicted to not completely vaporize even for flame conditions when the engine speed is high.

In the discussion on cold-starting, it was suggested that increasing the compression ratio helps fuel spray evaporation, but an increase from 9.3:1 to 12:1 only increased estimated fuel evaporation a small amount. However, the increased compression ratio possible with high-octane alcohol fuels helps predicted efficiency significantly. Table 3 shows a comparison of engine performance at the road-load condition discussed in the previous paragraph for n-heptane, ethanol, and methanol at a compression ratio of 9.3:1, and then for ethanol and methanol at a compression ratio of 12:1. For all cases, the fueling is stoichiometric. Note that the calculations were based on constant intake and exhaust manifold pressure, rather than constant power. For calculations at constant power, as the power increases with increasing compression ratio or reduced compression work with the alcohol fuels, the throttle would have to be closed, increasing pumping losses. These engine efficiency calculations were based on computed pumping losses, compression losses including cylinder pressure reductions resulting from cooling in evaporating the liquid fuel, estimated burning rates using a Wiebe function, and friction losses based on typical spark ignition engines, but not including the additional frictional losses associated with the increase in compression ratio. In fact, the increase in frictional losses and heat transfer with increasing compression ratio typically limits the compression ratio for maximum thermal efficiency with a spark ignition engine to about 17 (Heywood 1988).

The improvements in efficiency associated with the alcohol fuels appear high relative to results reported elsewhere. Heywood (1988) suggests that efficiency increases about 3% per unit increase in compression ratio. These calculations of efficiency are based on energy content of the fuel, which is lower for the alcohols than for n-heptane. The calculations do not account for the effect of the increased fuel weight and fuel tanks for the alcohol fuels. However, it appears that using alcohol fuels in an engine with a compression ratio selected for gasoline results in a very significant loss in potential efficiency.

Summary and Conclusions

A new concept has been proposed for low-temperature, cold-starting, alcohol-fueled vehicles. The approach is to use fine-spray, port-fuel injectors to spray fuel directly from the injector into the cylinder, using the air flow into the cylinder to carry the fine spray. The spray drops are fine enough that they will

remain suspended in the air as it goes into the cylinder, in contrast to conventional port-fuel injectors that spray fuel onto the intake valve and port. In these conventional systems, it is mostly fuel vapor, not liquid fuel, that goes into the cylinder during cranking. To follow up on this new cranking and starting concept, fine-spray fuel injectors were developed, and a computer model was used to estimate the performance of fine alcohol fuel sprays in engines.

Air-assist caps for standard pintle or multi-hole port-fuel injectors were developed and tested on methanol (M100) fuels. These injectors exceeded the goal of producing sprays with SMDs less than 10 μm using air pressure differentials of 138 kPa (20 psid). Using a 1.4-mm exit hole diameter and 100 $kPa_{diff.}$ (15 psid) pressure differential from an air-assist injector cap, cross-section average SMDs of about 7.5 μm were produced with fuel-injection pulse widths of 4 ms (idle condition), and SMDs of 9 μm were produced with a 10-ms pulse width. Standard production PWM can be used to control these injectors, although the engine controller may need to account for air flow into the engine through the injector, depending on the engine control strategy.

A detailed spray evaporation model developed at SwRI, the TESS code, was combined with an engine cycle-simulation model to predict in-cylinder temperatures, pressures, evaporation rates, and combustion rates. Calculations of in-cylinder evaporation of methanol (M100) and ethanol (E100) were compared with a single-component simulation of gasoline, n-heptane, at cranking temperatures from -25°C to 25°C and at road-load condition. During cranking, the n-heptane produced a prevaporized combustible fuel-air mixture by TDC of the compression stroke for all temperatures, while the evaporation rates of ethanol and methanol were lower due to their higher latent heats of vaporization (n-heptane, 318 kJ/kg; ethanol, 963 kJ/kg; methanol, 1121 kJ/kg). At the highest temperature of 25°C, the alcohols could produce a prevaporized vapor-air combustible mixture; at the lowest temperature of -25°C, vaporization of the alcohols appeared too slow to get a prevaporized combustible mixture. However, it is proposed that if the fine spray could be kept suspended in the air, it may be possible to use direct-spark vaporization and combustion of the liquid drops. Engine tests are required to evaluate this concept.

The spray evaporation model indicates that evaporation rates for alcohol fuels increase with decreasing drop size until the spray SMD reaches about 10 μm. Further reductions in drop size do not increase evaporation rates because the alcohol fuel drops absorb the enthalpy of the air as fast as it is available for SMDs of 10 μm and smaller. Increases in compression ratio above the standard 9.3 value for the Ford 3-L engine help computed engine efficiencies, while increasing evaporation rates during cranking only slightly.

Recommendations for Future Work

1. One potential follow-on for this effort is to perform engine tests of the proposed concept of using fine-spray, port-fuel injectors with alcohol fuels to improve low-temperature cold-starting. A project to examine this approach for ethanol fuels already has been funded at SwRI, and further work efforts in this area are not required at this time.

2. The calculations of fuel evaporation rates as reported above give insight into fuel-spray evaporation during spark-ignition engine operation. However, the limitation to single-component fuels does not allow an examination of the effects of, for example, adding light-end petroleum fuels such as butane and pentane to alcohol fuels. Similarly, the effects of gasoline distillation curves on evaporation during a cycle cannot be examined using the existing model. Converting the TESS spray evaporation code to handle multi-component fuels would allow an evaluation of real fuel blends on evaporation rates.

3. The fuel being delivered to the cylinder of a spark-ignition engine using fine-spray injectors is a combination of the fine spray injected "directly" into the cylinder and the fuel vapor and liquid from

the portion of the fuel spray that impacts with the port walls and the intake valve(s). Accurately controlling the in-cylinder fuel-air ratio requires understanding all the sources of fueling, both direct from the injector and indirect from vapor off the walls and liquid traveling along the walls. SwRI has models for each of these individual fuel sources. These submodels should be combined into one model that predicts alcohol fuel delivery to the cylinder, for both methanol and ethanol, including fuel blends.

References

Dodge, L.G. (1988). "Representation of Average Drop Sizes in Sprays," *Journal of Propulsion and Power*, Vol. 4, No. 6., pp. 490-496.

Heywood, J.B. (1988). *Internal Combustion Engine Fundamentals*, New York: McGraw-Hill Publishing Co.

Jorgensen, S.W. (1988). "Compression Temperatures in a Cold Cranking Engine," SAE 880045, Warrendale, PA: Society of Automotive Engineers.

Siewert, R.W., and Groff, E.G. (1987). "Unassisted Cold Starts to -29° and Steady-State Tests of a Direct-Injection Stratified-Charge (DISC) Engine Operated on Neat Alcohols," SAE 872066, Warrendale, PA:. Society of Automotive Engineers.

Appendix A

TESS
(Trajectory and Evaporation of Spray Systems)
Spray Computer Model - Mathematical Background

For purposes of discussion, the TESS model is divided into three parts: (1) Thermodynamics, (2) Aerodynamics, and (3) Drop-Size Distributions and Average Drop Sizes. Each section is discussed in order. An overall flow chart is shown in Figure A-1.

Thermodynamics

This portion of TESS computes the heat-up of the drop, the final steady-state temperature, and the fuel and air properties necessary for those calculations. This portion of the model is very similar to that described by Chin and Lefebvre (1982, 1983) except that some of the fuel property data were taken from the American Petroleum Institute Data Book (Anon. 1970), and the properties of many fuels and liquids are contained in input files. The results from this model are very similar to those presented by Chin and Lefebvre when the model is used for quiescent fuel sprays. The integration of this part of the model with the other sections to be described allows the examination of sprays in situations where both spray and air are moving with a nonzero relative velocity. The mathematics are outlined below, based on the work of Chin and Lefebvre (1982, 1983), which in turn is based on the theories described by Spalding (1955).

The steady-state temperature is determined as follows. The mass transfer rate, m_j, from a drop is given by,

$$\dot{m}_f = 2\pi D \left(\frac{k_g}{c_{p,g}} \right) \ln(1+B) \tag{1}$$

where D is the diameter, k_g is the thermal conductivity of the gas, $c_{p,g}$ is the specific heat of the gas at constant pressure, and B is either B_M, the mass diffusion transfer number if mass diffusion is controlling, or B_T, the thermal diffusion transfer number if heat transfer is controlling, and the Lewis number is assumed to be unity. B_M is defined as:

$$B_M = \frac{(Y_{f,s} - Y_{f,\infty})}{(1 - Y_{f,s})} \tag{2}$$

where $Y_{f,s}$ and $Y_{f,\infty}$ are the fuel mass fractions at the drop surface and in the ambient air, respectively, and $Y_{f,s}$ is:

$$Y_{f,s} = \frac{P_{f,s}\, M_f}{(P_{f,s}\, M_f + (P - P_{f,s})\, M_a)} \tag{3}$$

where $P_{f,s}$ is the fuel vapor pressure at the drop surface, P is the ambient pressure, and M_f and M_a are the molecular weights of fuel and air, respectively. The vapor pressure was calculated using the method

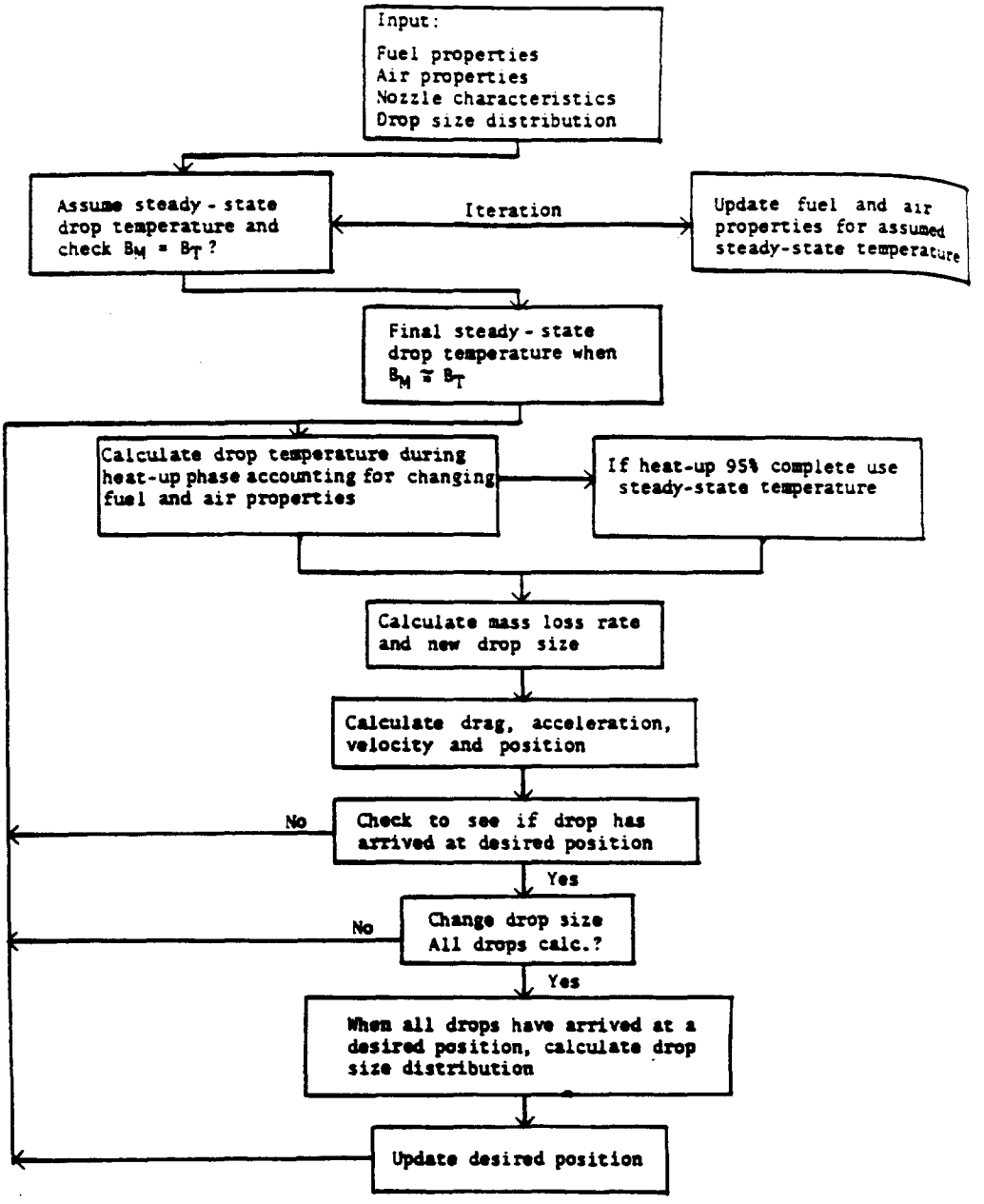

Figure A-1. TESS model flow chart

recommended by the American Petroleum Institute Data Book (Anon. 1970) called Procedure 5A1.10, "Vapor Pressure of Pure Hydrocarbons."

The thermal diffusion transfer number B_T for an evaporating drop is:

$$B_T = c_{p,g} \frac{(T_\infty - T_s)}{L} \tag{4}$$

where T_∞ and T_S are the ambient air temperature and drop surface temperature and L is the latent heat of fuel vaporization corrected from the normal boiling point to the actual surface temperature.

The accuracy of Eq. (1) is very dependent on the choice of values for k_g and $c_{p,g}$. As recommended by Chin and Lefebvre (1982), Sparrow's 1/3 averaging rule was used where a reference temperature was chosen as the drop surface temperature plus 1/3 of the difference between ambient air and surface temperatures. Similarly a reference value of the fuel vapor mass fraction, $Y_{v,r}$, was taken as the value just outside the surface plus 1/3 of the difference between the value at infinity and just outside the surface. The air mass fraction at the reference condition, $Y_{a,r}$ is then just $(1. - Y_{v,r})$. Using these reference conditions denoted by "r" the specific heat of the gas is given by,

$$c_{p,g} = Y_{a,r}\, c_{p,a\ (\text{at } T_r)} + Y_{v,r}\, c_{p,v\ (\text{at } T_r)} \tag{5}$$

and the thermal conductivity by,

$$k_g = Y_{a,r}\, k_{a\ (\text{at } T_r)} + Y_{v,r}\, k_{v\ (\text{at } T_r)} \tag{6}$$

At steady-state conditions, $B_M = B_T$ or from Eqs. (2) and (4)

$$\frac{Y_{f,s} - Y_{f,\infty}}{1 - Y_{f,s}} = \frac{c_{p,g}\,(T_\infty - T_{s,st})}{L} \tag{7}$$

where $T_{s,st}$ is the desired surface temperature under steady-state conditions. Assuming that the fuel vapor concentration in the ambient air is zero ($Y_{f,\infty} = 0$) and substituting for $Y_{f,s}$ from Eq. (3), then (7) becomes:

$$\frac{P}{P_{f,s}} - \frac{M_f}{M_a} \frac{L}{c_{p,g}\,(T_\infty - T_{s,st})} - 1 = 0 \tag{8}$$

In solving Eq. (8) to determine the steady-state surface temperature $T_{s,st}$, some of the variables can be specified, P, M_f, M_a, and T_∞ but the remaining three variables are functions of temperature, with L being related to the heat of vaporization at the normal boiling point $L_{T,bn}$ by,

$$L = L_{T,bn} \left[\frac{(T_{cr} - T_s)}{(T_{cr} - T_{bn})} \right]^{0.38} \tag{9}$$

where T_{cr} is the critical temperature and T_{bn} is the normal boiling point of the fuel. In order to solve Eq. (8) it is necessary to first assume a value for $T_{s,st}$. That temperature is used to calculate a reference

temperature T_r which in turn is used to calculate those quantities specified in Eqs. (5) and (6) used to calculate $c_{p,g}$ and k_g, and to calculate L as specified in Eq. (9). If the assumed value of $T_{s,st}$ is too low, the left side of Equation (8) will be positive. An iterative procedure must be used to continue specifying $T_{s,st}$ until Equation (8) is satisfied within the desired accuracy. That procedure results in a determination of the steady-state surface temperature $T_{s,st}$ and the transfer number $B=B_M=B_T$. The steady-state quiescent evaporation constant $\lambda_{q,st}$ can then be determined from,

$$\lambda_{q,st} = \frac{8\ k_g\ \ln(1+B)}{\rho_F\ c_{p,g}} \tag{10}$$

where ρ_F is the fuel density. Frossling (1938) has shown that convective effects can be accounted for in the case where heat transfer rates are controlling by,

$$\lambda_{c,st} = \lambda_{q,st}\ (1\ +\ 0.276\ Re_D^{0.5}\ Pr_g^{0.33}) \tag{11}$$

where $\lambda_{c,st}$ is the steady-state evaporation constant corrected for convective effects, Pr_g is the Prandtl number for the gas, and Re_D is the Reynolds number using the relative velocity between the drop and the gas. This velocity should include a fluctuating component in the case of turbulent flow. The fluctuating component of velocity may be set as a fraction of the axial velocity component, where the ratio is just the turbulence intensity. The default value of turbulence intensity is currently set in the source code to a value of 10% of the axial velocity. The effective velocity used to calculate Re_D for the evaporation calculation was taken as the sum of the fluctuating component (10% of the axial component of the air velocity) plus the difference between the drop and air velocities. These computations specify the steady-state properties of the drop.

The evaporation that occurs during the drop heat-up period is significant in many practical situations, with the drop being completely evaporated before reaching steady-state conditions in some instances. Chin and Lefebvre (1983) have predicted that high air pressures and convective effects both tend to increase the relative importance of the heat-up period relative to the steady-state phase of drop evaporation. For the general case, it is necessary to model the heat-up period in detail, and that is the approach used by TESS.

Chin and Lefebvre (1983) have shown that the rate of change of drop surface temperature is given by,

$$\frac{dT_s}{dt} = \left(\frac{\dot{m}_f\ L}{c_{p,f}\ m_f}\right)\left(\frac{B_T}{B_M} - 1\right) \tag{12}$$

where m_f is specified by Eq. (1) with $B=B_M$ during the heat-up period, and m_f is the drop (liquid phase) mass,

$$m_f = \left(\frac{\pi}{6}\right)\rho_f\ D^3 \tag{13}$$

The change of drop size with time is given by,

$$\frac{dD}{dt} = \frac{-4\ k_g\ \ln\ (1+B_M)}{\rho_f\ c_{p,g}\ D} \tag{14}$$

The drop temperature asymptotically approaches the steady-state temperature, and it was assumed that when the temperature had risen to 95% of the difference between the initial fuel temperature and the steady-state temperature, that the heat-up calculations could be terminated and steady-state properties used.

Aerodynamics

The approach used was a simplified version of the one developed at the University of Sheffield and described in several papers, e.g., Boyson and Swithenbank (1979). A cylindrical coordinate system was used where x is the axial distance, y the radial distance, and z the angular position, with corresponding velocities in the axial (u), radial (v), and tangential (w) directions.

The equations of motion of a particle (drop) neglecting all forces except drag, F, are,

$$\dot{u}_p = -F\ (u_p - u_\infty) \tag{15}$$

$$\dot{v} = \frac{w_p^2}{y_p} - F\ (v_p - v_\infty) \tag{16}$$

$$\dot{w} = \frac{v_p\ w_p}{y_p} - F\ (w_p - w_\infty) \tag{17}$$

where the "p" subscripts refer to the particle and the "∞" subscript refers to the free stream, and F is given by,

$$F = \left(\frac{18\ \mu_g}{\rho_p\ D^2}\right)\left(\frac{C_D\ Re_D}{24}\right) \tag{18}$$

where μ_g is the gas viscosity, ρ_p is the particle density, D is the particle diameter, C_D is the drag coefficient, and Re_D is the Reynolds number defined as,

$$Re_D = \frac{D_p\ \rho_g}{\mu_g}\ |\vec{u}_p - \vec{u}_\infty| \tag{19}$$

The drag coefficient, C_D, is given by Dickerson and Schuman (1965) as,

$$\begin{aligned} C_D &= 27\ Re_D^{-0.84} && 0 \le Re_D \le 80 \\ C_D &= 0.271 Re_D^{0.217} && 80 < Re_D \le 10^4 \\ C_D &= 2.0 && 10^4 < Re_D \end{aligned} \tag{20}$$

The equations of motion (Eqs. 15 to 17) are solved numerically using a step size of 1 to 10 μs, and the equations of trajectory are solved in a similar manner,

$$\dot{x}_p = u_p \tag{21}$$

$$\dot{y}_p = v_p \tag{22}$$

$$\dot{z}_p = \frac{w_p}{y_p} \tag{23}$$

These equations describe the trajectory of a particle in a gas stream. For each iteration in the trajectory calculation, the drop size and temperature are updated using the procedure described in the Thermodynamics section.

At the end of each iteration through the trajectory calculations, the current calculated axial position of the particle (or elapsed time) is checked against a target value. When the particle reaches that target value for axial position (or elapsed time), the position, transit time, size, temperature, and other parameters for that drop are frozen and the calculations are repeated for the next larger drop size. After all the drops each reach a targeted axial position, corresponding to a measurement location (or elapsed time), the drop size distribution is calculated, results are printed out, the target position (or time) is moved downstream (or later), and the calculations are repeated.

Drop-Size Distributions and Average Drop Sizes

Instrument Sampling Effects

Spray characteristics such as drop velocities change because of drag forces, and drop sizes change because of evaporation. Perhaps less obviously, the average drop sizes and velocities change depending on how the sizes and velocities are measured, even for error-free measurements. To illustrate this instrument sampling effect, consider an atomizer that produces 10 drops per second of 10 μm drops, and 10 drops per second of 100 μm drops. Assume the drops have an initial velocity of 10 m/s, but are sprayed into co-flowing air at 1 m/s. Because of aerodynamic drag, the smaller 10 μm drops rapidly decelerate to the air velocity, while the larger 100 μm drops, having 1000 times the mass of the 10 μm drops, maintain their momentum much longer and slow down toward the air velocity much less rapidly.

Ignore drop evaporation and consider the measurement of average drop sizes at a downstream location. If a photograph is taken of the spray at some downstream location, then the number of 10 μm drops in the picture will be much larger than the number of 100 μm drops because the smaller drops have slowed down more, and the average size (based on arithmetic mean) will be much less than 55 μm (Dodge et al. 1987). However, if the number of drops crossing a plane downstream of the injector is measured, both the 10 μm and 100 μm drops will cross the plane at a rate of 10 per second, and the average size (based on arithmetic mean) will be exactly 55 μm (Dodge et al. 1987). The crossing rate is the same for the small and large drops because, although the small drops are moving at a lower velocity, they are also more closely spaced, and thus the rate at which they cross a plane is constant (i.e., is a conserved quantity, Dodge et al. 1987). In the first case, average drop sizes are calculated based on the population of drops in a volume, called a number-density-weighted (NDW) average. In the second case, average drop sizes are calculated based on the flux of drops through a measurement plane, called a number-flux-weighted (NFW) average. Spray drop-sizing instrumentation samples in one of these two modes, either NDW or NFW, and results, even if performed without error, are typically different just as in the example cited above because of the correlation of drop velocities with drop sizes (Dodge et al. 1987; Dodge 1988).

Table A-1. Classification of Sampling Mode for Some Particle Sizing Equipment

Number-Density-Weighted Sampling Instruments	Number-Flux-Weighted Sampling Instruments
Laser-Diffraction (e.g., Malvern)	Phase-Doppler (e.g., Aerometrics, Dantec)
Imaging (e.g., photography, video imaging, PMS OAP 2-D, Bete Imaging)	Single-particle scattering intensity (e.g., PMS FSSP, Insitec single particle counter)
Photon correlation spectroscopy	All single-particle counting instruments

To make comparisons with experimental measurements easy, the TESS code computes size distributions and average drop sizes as both a NDW average, and a NFW average. This allows for a direct comparison with experimental measurements by instruments such as Malvern laser-diffraction or imaging instruments with the NDW averages, or measurements with instruments such as an Aerometrics Phase-Doppler or a PMS FSSP instrument with the NFW averages. Table 1 gives some guidelines as to the sampling modes of various types of drop-sizing equipment. Both NDW and NFW averages are provided if the calculations are made as a function of axial distance from the injector, where those same axial locations may be chosen to coincide with measurement locations. The TESS code may also be run in a mode where the spray is examined as a function of time rather than as a function of axial location. In this case, all drops are stopped at specified increments of time, and for this case, the drop size averages are presented only as NFW averages, since these are conserved in time while the NDW averages are not.

Average Drop Sizes

TESS makes all calculations on individual drops of certain sizes, using about 20 discrete size classes to represent the spray. The largest drop size available in the program is 4000 μm, but the largest size drop considered in a given calculation is based on the actual drop size distribution input, and is set to the smallest discrete drop size in the model for which less than 0.1% of the liquid volume fraction of the spray is contained in drops of larger sizes.

Although the TESS calculations consider the evaporation of a number of different sized drops, it is often easier to show trends of spray behavior based on average drop size plus a parameter to describe the spread in drop sizes rather than detailed data on every size class. The preferred definition of average drop size varies with the technical field of interest, but is rarely the arithmetic mean that is used as an average in other fields. The arithmetic mean is weighted toward the large number of very small drops in a spray, and most technical fields are more interested in a volume or surface area weighted average. In addition, the "smallest drop," or drop size for which only 10% of the spray volume is contained in drops of smaller size, or the largest drop for which only 10% of the spray volume is contained in drops of larger size are often of interest. One way of specifying the breadth of the drop size distribution is based on this largest drop size minus the smallest drop size, normalized by the median drop size. The average drop sizes computed by TESS include the Sauter mean diameter (SMD or D_{32}) and the volume median diameter, the 10% by volume diameter ($D_{V0.1}$) and the 90% by volume diameter ($D_{V0.9}$). These are calculated as follows.

The SMD is also called the surface area-volume mean diameter, and is defined as,

$$SMD \equiv D_{32} \equiv \frac{\sum_i n_i D_i^3}{\sum_i n_i D_i^2} \tag{24}$$

where n_i is the number of drops of size D_i.

The volume median diameter, $D_{V0.5}$ is that diameter for which 50% of the spray volume is contained in drops smaller than that diameter. If R(D) is the cumulative fraction of the spray volume (or spray mass) smaller than size D, then volume median diameter is defined by,

$$R(D_{V0.5}) = 0.5 \tag{25}$$

Similarly, the 10% by volume diameter, $D_{V0.1}$, and the 90% by volume diameter, $D_{V0.9}$, are defined based on the cumulative function R(D) by,

$$\begin{aligned} R(D_{V0.1}) &= 0.1 \\ R(D_{V0.9}) &= 0.9 \end{aligned} \tag{26}$$

Drop-Size Distributions

It is often convenient to assume a form of a statistical distribution for the fraction of spray volume as a function of drop size. Two distribution functions commonly used are log-normal and Rosin-Rammler. The TESS model currently allows for specification of the original drop size distribution at the injector tip as a Rosin-Rammler distribution. As the spray leaves the injector tip and progresses in time and distance and begins evaporation, it no longer follows exactly a Rosin-Rammler distribution. However, the model does calculate the best fit Rosin-Rammler distribution as the spray progresses in time and space at a given measurement location or a specified elapsed time from leaving the injector. To compare the predictions from the computer model with the experimental results, it is necessary to convert the computer predicted drop sizes at a given location into an equivalent set of two parameters specifying the Rosin-Rammler distribution.

If R(D) represents the fraction of the liquid being sprayed contained in drops larger than diameter D, then for the Rosin-Rammler distribution (Allen 1981),

$$R(D) = \exp\left(-\left(\frac{D}{X}\right)^N\right) \tag{27}$$

where X represents a size, and N specifies the width of the distribution. It is convenient to specify a spray by a single parameter representing an "average" drop size. However, a straight numerical average is heavily weighted toward the smallest drops, which are extremely plentiful but which contain a very small fraction of the total volume of the liquid. For combustion processes, the surface-to-volume ratio is important to evaporation, so an average drop size may be chosen which has a surface-to-volume ratio representative of the actual spray, and such an average is called the surface-volume mean diameter or SMD. The SMD is related to the Rosin-Rammler parameters by (Allen 1981),

$$SMD = \frac{X}{\Gamma}\left(1-\frac{1}{N}\right) \qquad N > 1 \tag{28}$$

Specifying X and N allows the calculation of the SMD, or specifying SMD and N determines X.

An initial set of drop sizes distributed approximately exponentially in size (i.e., evenly spaced when plotted as ln D) and covering the range of about 2 μm to 4000 μm with 20 different sizes is used in the model. Assuming size classes bounded by these drops as end points, the initial fraction of liquid contained in drops larger than a certain size class is given by,

$$\begin{aligned} R(D_i^0) &= \exp\left(-\left(\frac{D_i^0}{X}\right)^N\right) \qquad 1 \le i \le n \\ R(D_0^0) &= 1 \\ R(D_{n+1}^0) &= 0 \end{aligned} \tag{29}$$

where "n" is the number of drop size classes, D_i^0 is the initial drop diameter of the ith drop before evaporation, and the initial fraction of liquid in each size class is,

$$\begin{aligned} F_i^0 &= R(D_i^0) - R(D_{i+1}^0) \qquad 0 \le i \le n \\ F_{-1}^0 &= 0 \end{aligned} \tag{30}$$

After evaporation begins, the small drops begin evaporating quickly while the large ones evaporate slowly, changing the fraction of liquid in the different size classes unevenly. Denoting the smallest nonevaporated drop size by "k," the fraction of liquid remaining in any size class, F_i, is, for an NFW sample,

$$1F_i = \frac{F_i^0\left\{(D_i/D_i^0)^3/u_{p,i} + (D_{i+1}/D_{i+1}^0)^3/u_{p,i+1}\right\}/2}{\sum_{j=k}^{n} F_j^0\left\{(D_j/D_j^0)^3/u_{p,i} + (D_{j+1}/D_{j+1}^0)^3/u_{p,j+1}\right\}/2} \tag{31}$$

or, for an NDW sample,

$$F_i = \frac{F_i^0\left\{(D_i/D_i^0)^3 + (D_{i+1}/D_{i+1}^0)^3\right\}/2}{\sum_{j=k}^{n} F_j^0\left\{(D_j/D_j^0)^3 + (D_{j+1}/D_{j+1}^0)^3\right\}/2} \qquad k \le i \le n, \quad 0 \le k \le n \tag{32}$$

with the same limits for i and k as in Eq. 31, and where,

$$\begin{aligned} D_0 &= D_1 \\ u_{p,0} &= u_{p,1} \\ D_{n+1} &= D_n \\ u_{p,n+1} &= u_{p,n} \end{aligned} \tag{33}$$

and $u_{p,i}$ is the axial velocity of the ith drop, D_i is the instantaneous drop size, and D_i^0 is the initial drop size of the ith drop. Each size class is characterized by the drops making up the end points, and the initial fraction of liquid in a size class is modified by the average loss of volume of the end point drops. The

velocity term is added for the NDW sample to account for the fact that as the drops slow down, they increase their relative concentration, and thus their weighting factor in the NDW sample volume. Note that as u_p approaches zero, the NDW average becomes unstable. This is not a mathematical anomaly. Rather it is direct evidence for the need to make drop size measurements with NDW sampling instruments (e.g., laser-diffraction, video) only with co-flowing air, never into stagnant air. Otherwise, small drops may come to rest in the sampling volume, and the measurements would have an extreme bias to those small drops.

The cumulative fraction of liquid in all size classes including and larger than the ith class is,

$$R(D_i) = \sum_{j=i}^{n} F_i \qquad k \le i \le n \tag{34}$$

This instantaneous value of R_i is related to the drop sizes and Rosin-Rammler parameters by Eq. (29) with the initial drop size D_i^0 replaced by the instantaneous value D_i,

$$R(D_i) = \exp\left(-\left(\frac{D_i}{X}\right)^N\right) \qquad k \le i \le n \tag{35}$$

Taking the natural logarithm of both sides twice and excluding i=k (i.e., R_k=1), Eq. (35) becomes,

$$\ln_e\left(\ln_e\left(\frac{1}{R(D_i)}\right)\right) = N \ln_e D_i - N \ln_e X \qquad k+1 \le i \le n \tag{36}$$

This has the form of the equation of a straight line, y = mx + b, if the following definitions are used,

$$\begin{aligned} y &\equiv \ln_e(\ln_e(1/R(D_i))) \\ m &\equiv N \\ x &\equiv \ln_e D_i \\ b &\equiv -N \ln_e X \end{aligned} \tag{37}$$

Thus, by determining a least squares fit of the straight line through the data $\ln_e(\ln_e(1/R_i))$ versus $\ln_e D_i$, the Rosin-Rammler parameters are given by,

$$N = m \text{ (the slope)} \tag{38}$$

and

$$X = \exp\left(\frac{-b}{N}\right) \tag{39}$$

A standard routine is used to perform the least squares operation and the Rosin-Rammler parameters and the SMD [from Eq. (28)] are determined at each target value of the axial location corresponding to the position where experimental data are obtained. Although the initial distribution at the nozzle is an ideal Rosin-Rammler distribution, the distribution downstream does not correspond exactly to the Rosin-Rammler equation because of the different evaporation rates for the different sized drops, and the degree of fit is determined by the correlation coefficient of the straight line through the computed data.

References

Allen, T. (1981). *Particle Size Measurement*, Third Edition, London and New York: Chapman and Hall, pp. 139, 140.

Anon. (1970). *Technical Data Book - Petroleum Refining, Second Edition*, Washington, DC: American Petroleum Institute, Division of Refining.

Boyson, F., and Swithenbank, J. (1979). "Spray Evaporation in Recirculating Flow," Seventeenth Symposium (International) on Combustion, The Combustion Institute, pp. 443-453.

Chin, J.S., and Lefebvre, A.H. (1982). "Steady State Evaporation Characteristics of Hydrocarbon Fuel Drops," AIAA-82-1176, presented at the American Institute of Aeronautics and Astronautics/Society of Automotive Engineers/American Society of Mechnical Engineers 18th Joint Propulsion Conference.

Chin, J.S., and Lefebvre, A.H. (1983). "The Role of the Heat-Up Period in Fuel Drop Evaporation."

Dickerson, R.A., and Schuman, M.D. (1965). "Rate of Aerodynamic Atomization of Droplets," *Journal of Spacecraft and Rockets*, pp. 99-100.

Dodge, L.G., Rhodes, D.J., and Reitz, R.D. (1987). "Drop-Size Measurement Techniques for Sprays: Comparison of Malvern Laser-Diffraction and Aerometrics Phase-Doppler," *Applied Optics*, Vol. 26, No. 11, pp. 2144-2154.

Dodge, L.G. (1988). "Representation of Average Drop Sizes in Sprays," *Journal of Propulsion and Power*, Vol. 4, No. 6, pp. 490-496.

Frossling, N. (1938). "On the Evaporation of Falling Droplets," *Gerlands Beitrage zur Geophsik*, Vol. 52, pp. 170-216.

Spalding, D.B. (1955). *Some Fundamentals of Combustion*, London: Butterworths Scientific Publications.

REPORT DOCUMENTATION PAGE

Form Approved
OMB NO. 0704-0188

1. AGENCY USE ONLY (Leave blank)	2. REPORT DATE	3. REPORT TYPE AND DATES COVERED
	June 1994	Subcontract report

4. TITLE AND SUBTITLE

Injector Spray Characterization of Methanol in Reciprocating Engines

5. FUNDING NUMBERS

(C) AW-2-12266-1
(TA) FU421010

6. AUTHOR(S)

L. Dodge and D. Naegeli

7. PERFORMING ORGANIZATION NAME(S) AND ADDRESS(ES)

Southwest Research Institute
San Antonio, Texas 78228-0510

8. PERFORMING ORGANIZATION REPORT NUMBER

DE94006948

9. SPONSORING/MONITORING AGENCY NAME(S) AND ADDRESS(ES)

National Renewable Energy Laboratory
1617 Cole Boulevard
Golden, CO 80401-3393

10. SPONSORING/MONITORING AGENCY REPORT NUMBER

NREL/TP-425-6344

11. SUPPLEMENTARY NOTES

12a. DISTRIBUTION/AVAILABILITY STATEMENT

National Technical Information Service
U.S. Department of Commerce
5285 Port Royal Road
Springfield, VA 22161

12b. DISTRIBUTION CODE

UC-335

13. ABSTRACT *(Maximum 200 words)*

This report covers a study that addressed cold-starting problems in alcohol-fueled, spark-ignition engines by using fine-spray port-fuel injectors to inject fuel directly into the cylinder. This task included development and characterization of some very fine-spray, port-fuel injectors for a methanol-fueled spark-ignition engine. After determining the spray characteristics, a computational study was performed to estimate the evaporation rate of the methanol fuel spray under cold-starting and steady-state conditions.

14. SUBJECT TERMS

Methanol, methanol fuel spray, alcohol fuel, reciprocating engines

15. NUMBER OF PAGES

56

16. PRICE CODE

A04

17. SECURITY CLASSIFICATION OF REPORT	18. SECURITY CLASSIFICATION OF THIS PAGE	19. SECURITY CLASSIFICATION OF ABSTRACT	20. LIMITATION OF ABSTRACT